UNCLASSIFIED

SECURITY CLASSIFICATION OF THIS PAGE

REPORT DOCUMENTATION PAGE

1a. REPORT SECURITY CLASSIFICATION UNCLASSIFIED	1b. RESTRICTIVE MARKINGS
2a. SECURITY CLASSIFICATION AUTHORITY	3. DISTRIBUTION/AVAILABILITY OF REPORT Approved for public release; distribution unlimited.
2b. DECLASSIFICATION/DOWNGRADING SCHEDULE	
4. PERFORMING ORGANIZATION REPORT NUMBER(S) AFWAL-TR-84-3109	5. MONITORING ORGANIZATION REPORT NUMBER(S)
6a. NAME OF PERFORMING ORGANIZATION Flight Dynamics Laboratory AFWAL/FIMG 6b. OFFICE SYMBOL (If applicable) AFWAL/FIMG	7a. NAME OF MONITORING ORGANIZATION
6c. ADDRESS (City, State and ZIP Code) Flight Dynamics Laboratory (AFWAL/FIMG) AF Wright Aeronautical Laboratories (AFSC) Wright-Patterson AFB, OH 45433	7b. ADDRESS (City, State and ZIP Code)
8a. NAME OF FUNDING/SPONSORING ORGANIZATION 8b. OFFICE SYMBOL (If applicable)	9. PROCUREMENT INSTRUMENT IDENTIFICATION NUMBER
8c. ADDRESS (City, State and ZIP Code)	10. SOURCE OF FUNDING NOS. PROGRAM ELEMENT NO. 24040751 / PROJECT NO. 2404 / TASK NO. 07 / WORK UNIT NO. 51
11. TITLE (Include Security Classification) Post-Stall Maneuvers and Thrust Vectoring Perf. Analysis (U)	
12. PERSONAL AUTHOR(S) L. Earl Miller	
13a. TYPE OF REPORT Final Technical Report 13b. TIME COVERED FROM Aug 83 TO Jul 84	14. DATE OF REPORT (Yr., Mo., Day) July 1984 15. PAGE COUNT 77
16. SUPPLEMENTARY NOTATION	
17. COSATI CODES FIELD / GROUP / SUB. GR.	18. SUBJECT TERMS (Continue on reverse if necessary and identify by block number)

19. ABSTRACT (Continue on reverse if necessary and identify by block number)

Post Stall Maneuvers (PSM) occur whenever the angle of attack exceeds the stall angle of attack. This effort addresses both instantaneous turning performance and minimum time turns. The analysis includes vectored and nonvectored thrust and steady state aerodynamics. For optimal instantaneous turning and nonvectored thrust, angles of attack approaching ninety degrees are employed when the speed approaches zero. For vectored thrust, the optimal controls are the stall angle of attack and the thrust vector angle equal to the complement of the angle of attack. From an instantaneous turning standpoint, the turning rates are comparable, but the deceleration is larger for vectored thrust relative to nonvectored thrust. For minimum time turns, PSM is optimal for both vectored and nonvectored thrust.

20. DISTRIBUTION/AVAILABILITY OF ABSTRACT UNCLASSIFIED/UNLIMITED ☒ SAME AS RPT. ☐ DTIC USERS ☐	21. ABSTRACT SECURITY CLASSIFICATION
22a. NAME OF RESPONSIBLE INDIVIDUAL L. EARL MILLER	22b. TELEPHONE NUMBER (Include Area Code) 513-255-2021 22c. OFFICE SYMBOL AFWAL/FIMG

DD FORM 1473, 83 APR EDITION OF 1 JAN 73 IS OBSOLETE.

SECURITY CLASSIFICATION OF THIS PAGE

FOREWORD

This report was prepared by Dr. Earl Miller of the High Speed Aero Performance Branch, Aeromechanics Division, Air Force Flight Dynamics Laboratory, Air Force Wright Aeronautical Laboratories, Wright-Patterson Air Force Base, Ohio. This research was accomplished under job order number 24040751, "Multiple Vehicle Air-to-Air Combat Applications." This effort was conducted during the period from August 1983 to July 1984.

The assistance of the Technical Review Committee is gratefully acknowledged. There criticisms, suggestions, and comments have significantly improved the quality of this report. The committee consisted of Dr. Wilbur Hankey, chairman, Colonel Jim Lang, presently Avionics Laboratory commander and formerly Flight Controls Division Chief, Mr. Tom Cord from the Flight Controls Division, and Mr. David Johnson Performance Group Chief. Also, the generous recommendations of Professor N. X. Vinh from the Aerospace Engineering Department at the University of Michigan and Professor Jason Speyer from the Department of Aerospace Engineering and Engineering Mechanics at the University of Texas are gratefully acknowledged.

TABLE OF CONTENTS

LIST OF FIGURES

LIST OF FIGURES (Cont'd)

LIST OF SYMBOLS

A,B	turning rate parameters
C_A	axial force coefficient
C_D	aerodynamic drag coefficient
C_L	aerodynamic lift coefficient
C_N	normal force coefficient
C_0	Hamiltonian function value
D	aerodynamic drag
D'	normalized drag
F_T, F_N	normalized forces
g	acceleration of gravity
H	Hamiltonian function
L	aerodynamic lift
L'	normalized lift
n	normal load factor
N	normal force
N'	normalized normal force
P_u,P_ψ,P_γ	costate variables
P,P_R	costate functions
q	dynamic pressure
S	aerodynamic reference area
T	thrust
T'	normalized thrust
u	nondimensional speed

LIST OF SYMBOLS (Cont'd)

V	speed
W	weight
x,y,z	coordinates
α	angle of attack
ϵ	$\alpha+\delta_v$
γ	flight path angle
δ	bank angle function
δ_v	thrust vector angle
λ_T,λ_N	acjoint functions
ρ	atmospheric density
σ	bank angle
τ	nondimensional time
ψ	heading angle
ω	turning rate function

Subscripts

max	maximum value
min	minimum value
$( )_\alpha$	derivative of ( ) with respect to angle of attack
CRIT	critical value
nom	nominal value
0	initial value
f	final value
STALL	aerodynamic stall Superscripts

Superscripts

$*$	optimal value

SECTION 1

INTRODUCTION

The purpose of this investigation is to determine the performance payoff of post stall maneuvering (PSM), sometimes called supermaneuverability, and thrust vectoring. PSM involves maneuvering at high angles of attack, angles greater than that for maximum lift coefficient. There are two potential PSM advantages. The first is the ability to rapidly change the flight path of the vehicle. The second is to obtain the larger pointing angles which is important from a weapon's standpoint. Pointing will not be addressed in this effort, but clearly it has an advantage at any speed.

In the past, conventional maneuvers were restricted to less than maximum lift angles of attack. If PSM has any advantage, it must be able to develop velocity rotational rates greater than that for conventional maneuvers. One way of addressing the PSM issue is by solving instantaneous turning performance and minimum time to turn problems. That is the approach that will be taken here. The analysis will be limited to subsonic speeds. The reason for this is that past performance studies have shown that if there is a performance payoff for PSM, then it occurs at low speeds; that is speeds below the corner velocity.

The first group of problems will be instantaneous turning performance problems. Thrust vectoring will be included. The solution to this problem yields insight into both the effect of thrust vectoring and high angle of attack maneuvers along the trajectory. The last problem is the variable speed optimal control problem for minimum time turns. The significance of this problem is that the effect of high angle of attack on drag as well as lift during accelerated maneuvers can be addressed.

An important difficulty with high angle of attack maneuvers is the ability to control the vehicle. This issue will not be addressed in this study. It will be assumed that the vehicle can be controlled anywhere between zero and ninety degrees angle of attack. This assumption should be addressed on its own since it relates to a critical problem area in achieving PSM capability.

Several papers (References 1-5) have focused attention on minimum time turns for high speed aircraft. These efforts include both two and three dimensional trajectories. The former correspond to constant altitude or vertical plane maneuvers, either split-S or half loops. In the next section, the equations of motion and the control constraints are presented.

SECTION II

PROBLEM FORMULATION

The coordinate system selected for the trajectory problems is a velocity coordinate frame. The definition of the velocity vector using a velocity coordinate frame includes the magnitude of the velocity, the heading angle, and the flight path angle. The rate equation for these variables are

$$\dot{V} = g(F_T - \sin\gamma) \tag{1}$$

$$\dot{\gamma} = \frac{g}{V}(F_N\cos\sigma - \cos\gamma) \tag{2}$$

$$\dot{\psi} = \frac{g}{V} F_N \frac{\sin\sigma}{\sin\gamma} \tag{3}$$

where

$$F_T = T' \cos(\alpha+\delta_v) - D' \tag{4}$$

$$F_N = T' \sin(\alpha+\delta_v) + L' \tag{5}$$

$$T' = T/W,\ D' = D/W,\ L' = L/W = n \tag{6}$$

The aerodynamic and propulsive forces are illustrated in Figure 1. The thrust is a function of throttle setting, Mach number, and altitude. The lift and drag are functions of Mach number, altitude, and the angle of attack. The position of the vehicle is determined from the kinematic relations

$$\dot{x} = V\cos\gamma\cos\psi \tag{7}$$

$$\dot{y} = V\cos\gamma\sin\psi \tag{8}$$

$$\dot{z} = V\sin\gamma \tag{9}$$

The change in the mass will be neglected. The constraints for these equations are

$$n \leq n_{max} \tag{10}$$

$$T_{min} \leq T \leq T_{max} \tag{11}$$

For this study minimum thrust is zero. There are four controls for this situation. The propulsion controls are the thrust magnitude, T, and thrust vector angle, δ_v. The aerodynamic controls are the aerodynamic angle of attack, α, and bank angle, σ. Since the study has application to post stall maneuvering, the angle of attack is limited only by the maximum value of the structural load factor and ninety degrees. In previous studies it was limited to the stall angle of attack, α_{stall}. If the speed is greater than the corner speed, then the angle of attack is limited by the maximum value of the load factor. The corner speed occurs at the juncture between the $C_{L_{max}}$ and n_{max} limits. It is determined from

$$\frac{1}{2}\rho S C_{L_{max}} V_C^2 = n_{max} W \tag{12}$$

In the next section, instantaneous turning performance problems are addressed.

SECTION III

INSTANTANEOUS TURNING PERFORMANCE

Instantaneous turning performance corresponds to point performance analysis. Each point in the flight envelope can be studied independently of every other point. In Section IV where continuous turning performance is studied, it is proven that for minimum time turns the optimal trajectory is in the vertical plane. Therefore, this section will consider only vertical plane trajectories. The appropriate turning rate equation is the time rate of change of the flight path angle

$$\dot{\gamma} = \frac{g}{V}(F_N \cos\sigma - \cos\gamma) \tag{13}$$

where

$$F_N = T' \sin(\alpha+\delta_V)+L' \tag{14}$$

The bank angle σ is zero or 180 degrees (0° corresponds to a pull up and 180° corresponds to a pull down). Introduce the turning rate function ω defined by

$$\omega = \frac{g}{V} F_N \tag{15}$$

The actual flight path angular rate is related to ω as follows

$$\dot{\gamma} = \omega\cos\sigma - \frac{g}{V}\cos\gamma \tag{16}$$

At any point on the trajectory, that is given the speed, flight path angle, and the altitude, the objective is to determine the propulsive and aerodynamic controls that optimize the flight path angular rate. This includes both maximizing and minimizing $\dot{\gamma}$. This is accomplished by optimizing the turning rate function ω.

The maximum of $\dot{\gamma}$ corresponds to $\sigma = 0$ and maximum ω. Minimum $\dot{\gamma}$ corresponds to $\sigma = \pi$ and maximum ω. Thus in both cases, the limits result from maximum ω. From Equation (15) it follows that maximum ω results from maximizing F_N. Clearly maximum thrust maximizes F_N. The rest of the section will concentrate on maximizing the turning rate function ω.

Aerodynamic Relations

Typical aerodynamic data from Reference 6 are illustrated in Figures 2 and 3, and correspond to the F15 which is a high performance fighter. The data represent steady state aerodynamics. Non steady, or time dependent, aerodynamic lift data are superimposed on top of the steady state data in Figure 4. The non steady data are only an illustration of a phenomena called dynamic overshoot and undershoot. When the rate of change of the angle of attack is very large, the available lift first exceeds the steady state lift. After the stall angle of attack is reached, there is a rapid transition from overshoot to undershot where the lift decreases with angle of attack. When the angle of attack is rapidly reduced, the dynamic lift drops below the steady state values. The overshoot and undershoot aerodynamics are not completely understood to say the least, therefore, there is uncertainty in their prediction. There is some understanding of the variables involved, however. The overshoot is primarily a function of $\dot{\alpha}$ and the final value of α. The transition from overshoot to undershoot is time dependent and the lift may be asymmetric, one wing may stall before the other. The undershoot depends on the value of maximum C_L in overshoot and is also time dependent. The drag also experiences variations from the steady state values. The drag may lag the non steady lift. For the rest of this effort, we will consider only steady state aerodynamics.

The normal and axial force coefficients are related to the lift and drag coefficients and the angle of attack in the following way

$$C_N = C_L\cos\alpha + C_D\sin\alpha \quad (17)$$

$$C_A = C_D\cos\alpha - C_L\sin\alpha \quad (18)$$

The steady state data correspond to subsonic Mach numbers. It will be assumed throughout this effort that the Mach numbers are sufficiently low that Mach number effects can be neglected. The coefficients that correspond to the data of Figures 2 and 3 are presented in Figure 5. From these data, approximate relations can be deduced for use in performance prediction

$$C_A = 0 \quad (19)$$

$$\begin{aligned} C_N &= 0.16+3.44\alpha && 0 < \alpha < 0.44 \text{ rad} \\ &= -1.72+12.04\alpha-9.86\alpha^2 && 0.44 < \alpha < 0.61 \text{ rad} \\ &= 1.96 && 0.61 < \alpha \end{aligned} \quad (20)$$

The relations for the lift and drag coefficients reduce to

$$C_L = C_N\cos\alpha \quad (21)$$

$$C_D = C_N\sin\alpha \quad (22)$$

These equations are exact if C_A is exactly zero. They are in good agreement with the experimental data as can be seen by examination of Figures 2 and 3. The approximate relations are used in all subsequent calculations.

Angle of Attack Variations, $\delta_v = 0$

For no thrust vectoring, $\delta_v = 0$. For a given Mach number, T/W, and altitude, the turning rate looks like that illustrated in Figure 6. The turning rate has a maximum somewhere between 0 and 90 degrees angle of attack. Both the shape of the curve and the

location of the maximum value are sensitive to the Mach number. In Figure 7, ω is presented as a function of Mach number for constant values of the angle of attack. The latter varies from 0 to 90 degrees in 5 degree increments. For constant α, ω decreases with increasing Mach number until the minimum is reached. This minimum will be referred to as the critical speed. From there on ω increases through the subsonic region.

For a given Mach number, there is an angle of attack that gives maximum ω. At low Mach numbers the angle of attack is high and goes to 90 degrees as the Mach number goes to zero. At high Mach numbers the optimum angle of attack approaches that for α_{STALL}. This behavior can be seen by inspection of Equations (14) and (15). Optimization of Equation (14) with respect to the angle of attack requires that

$$T\cos\alpha + \frac{\partial L}{\partial \alpha} = T\cos\alpha + qSC_{L_\alpha} = 0 \qquad (23)$$

Since the first term is positive the second term must be negative. This can occur only for angles of attack greater than that for α_{STALL}. From Equation (21)

$$C_{L_\alpha} = C_{N_\alpha}\cos\alpha - C_N\sin\alpha \qquad (24)$$

Equation (23) becomes

$$T\cos\alpha + qS(C_{N_\alpha}\cos\alpha - C_N\sin\alpha) = 0 \qquad (25)$$

The optimum angle of attack, α^*, for a given speed and altitude is determined from

$$\tan\alpha^* = \frac{T + qSC_{N_\alpha}}{qSC_N} \qquad (26)$$

At low speeds, q is small and α^* approaches ninety degrees. At high speeds, q is large and α^* approaches α_{stall}. This conclusion is deduced from comparison with Equation (24). Equation (23) can be rewritten as follows

$$T\cos\alpha + L\frac{C_{L_\alpha}}{C_L} = 0 \tag{27}$$

Solving for L and substituting into Equation (15) gives

$$\omega_{max} = \frac{g}{V} T'\left(\sin\alpha^* - \frac{C_L^*}{C_{L_\alpha}^*}\cos\alpha^*\right) \tag{28}$$

In Figure 8 is illustrated the optimum angle of attack for altitudes of ten and twenty thousand feet. Also included, are the angles of attack corresponding to zero longitudinal acceleration and a load factor limit equal to 7.33. At speeds below the corner speed, the structural limit can not be reached. Also, at low speeds the maximum turning rate and the turning rate at $\dot{V} = 0$ and zero flight path angle are the same. The reason for this is the angle of attack is higher than that value where C_N reaches its maximum value. Since maximum turning rate corresponds to maximum F_N, from Equations (5) and (21)

$$F_N = T'\sin\alpha + N'\cos\alpha \tag{29}$$

$$\frac{\partial F_N}{\partial \alpha} = T'\cos\alpha - N'\sin\alpha + \frac{\partial N'}{\partial \alpha}\cos\alpha \tag{30}$$

But the last term is zero since C_N is constant. Comparison with Equation (4)

$$F_T = T'\cos\alpha - N'\sin\alpha \tag{31}$$

shows that

$$F_T = \frac{\partial F_N}{\partial \alpha} \tag{32}$$

Thus the angle of attack for maximum turning rate and $\dot{V} = 0$, $\gamma = 0$ are the same whenever the maximum occurs at an angle of attack where C_N is constant. Refer to the intersection between the two angle of attack curves as the equilibrium speed. The reason for calling it this is that the speed will not change once this point is reached because $\dot{V} = 0$. The only way the speed can decrease is if the angle of attack is increased creating more drag or the thrust is reduced. It can be concluded that if the initial speed is greater than the equilibrium speed and C_N is equal to $C_{N_{max}}$ the the vehicle declerates to the equilibrium speed and then remains there. If the flight path angle is not zero, then from Equations (1) and (4) the equilibrium speed is less (greater) than the zero flight path case if the flight path angle is positive (negative).

At higher speeds the structural limit comes into play. The speed at which this occurs increases with increasing altitude since the dynamic pressure decreases. Only the structural limit for ten thousand feet is shown since the corner speed at twenty thousand feet is greater than a Mach number of 0.6. The angle of attack for $\dot{V} = 0$, $\gamma = 0$ is less than that for maximum turning rate since the drag in Equation (4) increases with increasing speed. In order to satisfy $\dot{V} = 0$, the angle of attack must decrease with increasing speed. In Figure 9 are presented turning rates corresponding to the maximum, $\dot{V} = 0$ for $\gamma = 0$, and the structural limit at ten and twenty thousand feet. As the altitude increases, the thrust decreases for a given Mach number and the dynamic pressure decreases also. Consequently, optimum ω decreases.

Critical Speed, $\delta_V = 0$

The critical speed is that speed where the turning rate is minimum with respect to speed for a given angle of attack and

thrust. This is not to be confused with absolute minimum turning rate which corresponds to zero lift and zero thrust.

For a given angle of attack, Equation (15) and Figure 7 shows that ω varies with respect to V in the following manner

$$\omega = \frac{A}{V} + BV \tag{33}$$

where

$$A = gT\sin\alpha, \quad B = \frac{g\rho SC_L}{2W} \tag{34}$$

A and B are invariant with respect to the speed if the thrust does not vary with respect to the speed. If the thrust can be treated as a constant, then the minimum turning rate is determined from the minimum of Equation (33)

$$-\frac{A}{V^2} + B = 0 \tag{35}$$

or

$$T\sin\alpha = L \tag{36}$$

The critical speed, V_{CRIT}, is the solution of

$$V^2_{CRIT} = \frac{2T\sin\alpha}{\rho SC_L} \tag{37}$$

For low thrust, V_{CRIT} is low. For small angles of attack, $\sin\alpha$ is approximately α and C_L is approximately $C_{L_\alpha}\alpha$. Thus Equation (37) is approximately

$$V_{CRIT}^2 = \frac{2T}{\rho S C_{L_\alpha}} \tag{38}$$

The critical speed is independent of α. For high angles of attack, $\sin\alpha$ increases, C_L decreases and Equation (37) shows the critical speed increases. Figure 9 shows that the critical speed is approximately 0.15 Mach number. The equilibrium speed was approximately 0.2 Mach number. The minimum turning rate is obtained by substituting Equation (36) into Equation (15)

$$\omega_{min} = \frac{2g}{V} T' \sin\alpha \tag{39}$$

Thrust Magnitude Variations, $\delta_v = 0$

A sensitivity analysis with respect to maximum thrust variations was conducted. For an altitude of 20,000 feet, maximum turning rate is presented in Figure 10 for different thrust levels. T_{nom} corresponds to the nominal values used in the previous calculations. At low speeds the maximum turning rate is nearly linear with respect to the thrust. At high speeds the turning rate is essentially insensitive to the thrust since the lift dominates.

This behavior can be explained by examining Equation (28). At low speeds, α^* is large, thus approximately

$$\omega_{max} = \frac{g}{V} T' \tag{40}$$

Maximum turning rate varies linearly with the thrust. The situation at high speeds is explained as follows. Combining Equation (15), (21), and (26) gives after some manipulation

$$\omega_{max} = \frac{g\cos\alpha}{VN'} (T'^2 + N'^2 + T' N_\alpha') \tag{41}$$

where

$$N'_{\alpha} = \frac{qSC_{N_{\alpha}}}{W} \tag{42}$$

At high speeds, $C_{L_{\alpha}} = 0$, $N'_{\alpha} = N' \tan\alpha$, $N'^{2} >> T'^{2} N'^{2} >> T' N'_{\alpha}$, hence

$$\omega_{max} = \frac{g}{V} N' \cos\alpha^{*} \tag{43}$$

The maximum turning rate is relatively insensitive to thrust variations.

The sensitivity of the optimum angle of attack to variations in the thrust is presented in Figure 11. At low speeds where α^{*} is large, Equation (26) shows that $\tan\alpha$ varies linearly with the thrust. At high speeds, Equation (23) shows that $C_{L_{\alpha}}$ approaches zero. Hence α^{*} approaches α_{stall} which is independent of the thrust.

Aerodynamic Variations, $\delta_V = 0$

A sensitivity analysis of the influence of the maximum value of normal coefficient on the maximum turning rate was conducted. The variation in the aerodynamic normal force coefficient is a constant multiple of the values defined earlier. $C_{N_{nom}}$ data are the nominal values used earlier. Maximum turning rate is presented in Figure 12. The value of $C_N/C_{N_{nom}} = 2.0$ represents an extreme change in steady state aerodynamics. In unsteady flow, it may be possible to exceed this value. It is assumed that maximum

C_N is achieved at the same α_{stall}. It has been observed in experimental aerodynamics that α_{stall} varies. At low Mach numbers where the thrust dominates, turning rate is approximately

$$\omega = \frac{g}{V} T \tag{44}$$

and is insensitive to aerodynamic variations. At high Mach numbers where the lift dominates, the turning rate varies in a linear manner with respect to the maximum value of the normal force coefficient.

The explanation for this is as follows. At low speeds, α^* is large and approximately ninety degrees. Equation (28) shows that the maximum turning rate is insensitive to variations in C_N. At high speeds, Equation (43) shows that the maximum turning rate is proportional to the normal force.

The optimum angle of attack is presented in Figure 13. At low speeds, Equation (26) shows that α^* decreases with increasing $C_{N_{max}}$. At high speeds, α^* approaches α_{stall} which we assumed to be independent of maximum $C_{N_{max}}$ for this steady state aerodynamic data.

Thrust Angle Variations

The analysis of the influence of δ_v is next. In Figures 14 and 15 are presented the maximum turning rate and the corresponding angle of attack, respectively. The thrust angles vary from zero to sixty degrees in ten degree increments. The maximum turning rate is relatively insensitive to the thrust vector angle.

The optimum angle of attack for a given δ_v is obtained from Equations (15) and (24)

$$T\cos(\alpha+\delta_v)+qSC_{L_\alpha} = T\cos(\alpha+\delta_v)+qS(C_{N_\alpha}\cos\alpha-C_N\sin\alpha) = 0 \quad (45)$$

The optimum angle of attack is greater the α_{stall}. The optimum angle of attack, α^*, is the solution of

$$\tan\alpha^* = \frac{T\cos\delta_v+qSC_{N_\alpha}}{T\sin\delta_v+qSC_N} \quad (46)$$

This equation agrees with Equation (26) when $\delta_v = 0$. At low speeds where q is small,

$$\tan\alpha^* = \cot\delta_v \quad (47)$$

The solution is

$$\alpha^* = \frac{\pi}{2} - \delta_v \quad (48)$$

Since $T\sin(\alpha^*+\delta_v)$ dominates, from Equations (14) and (15) maximum ω is approximately

$$\omega_{max} = \frac{g}{V}T \quad (49)$$

At high speeds where q is large, Equation (45) shows that C_{L_α} must decrease and α^* therefore approaches α_{stall}. L dominates and

$$\omega_{max} = \frac{g}{V} L'_{max} \tag{50}$$

where

$$L'_{max} = qSC_{L_{max}}/W \tag{51}$$

The global maximum of the turning rate is obtained by maximizing simultaneously with respect to both the angle of attack and the thrust vector angle. Recall Equation (15)

$$\omega = \frac{g}{V} [T' \sin(\alpha+\delta_v)+L'] \tag{15}$$

The optimum is obtained by maximizing both terms. Thus, the angle of attack is that for $C_{L_{max}}$ and the thrust vector angle is the complement of the angle of attack. Hence

$$\omega_{max} = \frac{g}{V} (T' + L'_{max}) \tag{52}$$

This result can also be determined rigorously. In order for F_N to be maximized, it is necessary that the following equations be satisfied

$$\frac{\partial F_N}{\partial \alpha} = T' \cos(\alpha+\delta_v) + \frac{\partial L'}{\partial \alpha} = 0 \tag{53}$$

$$\frac{\partial F_N}{\partial \delta_v} = T' \cos(\alpha+\delta_v) = 0 \tag{54}$$

From the latter, the sum is ninety degrees. Substitution into the first equation shows that

$$\frac{\partial L'}{\partial \alpha} = 0 \qquad (55)$$

which occurs at α_{stall}.

In Figures 16 and 17, sustained turning rate and the corresponding angle of attack are presented. Comparison of Figures 14 and 16 shows that the angle of attack at low speeds is the same for maximum turning rate. Since C_N is nearly constant, Equation (45) reduces to Equation (4). Thus for zero flight path angle, the solution for maximum and sustained turns are the same. At high speeds, maximum turning occurs simultaneously with longitudinal deceleration. Thus, thrust vectoring will result in faster decelerations relative to the zero vector angle case. There is no equilibrium speed if thrust vectoring is used because for maximum turning rate $\alpha+\delta_v$ is ninety degrees and therefore F_T is the negative of the drag and $\dot{V}<0$.

PSM Versus Thrust Vectoring

In Figure 18, maximum turning rate is presented for optimal PSM and thrust vector maneuvers. In general, thrust vectoring gives slightly higher turning rates. The corresponding optimal angles of attack are presented in Figure 19. For thrust vectoring, α_{stall} is approximately 31.6 degrees and δ_v is 58.4 degrees. Longitudinal decelerations at zero flight path angle are presented in Figure 20. Thrust vectoring produces greater decelerations since the thrust component in Equation (4) is zero. Figures 18 and 20 illustrate that comparable turing performance can be achieved through PSM maneuvers or thrust vectoring.

Summary

Based strictly upon steady state aerodynamics, subsonic Mach numbers less than 0.6, and instantaneous point performance considerations, very high angles of attack (beyond stall) turns should be employed only at low speeds where the thrust dominates the lift. The situation is reversed at high Mach numbers where the angle of attack approaches the stall value. Increasing thrust gives higher turning rates particularly at low Mach numbers and increasing normal force coefficients increases the turning rates at high Mach numbers. The equilibrium Mach number (Mach number where maximum turning and zero rate deceleration at zero flight path angle are equal) is approximately 0.2. For pull ups the equilibrium speed decreases and it increases for pull down maneuvers. With thrust vectoring, the optimal angle of attack is α_{stall} and the optimal thrust vector angle is the complement of the angle of attack. This holds for all speeds. Hence post stall maneuvering (PSM) is not necessary for turning if thrust vectoring is available. Either optimal PSM maneuvers or thrust vectoring yield comparable turning performance.

Future studies should include the following aspects:

1. Unsteady aerodynamics
2. Analysis of aircraft pointing
3. Compare turning versus pointing
4. Air combat analysis MvN

SECTION IV

OPTIMAL VARIABLE SPEED MANEUVERING PERFORMANCE

It was demonstrated in the previous section on instantaneous turning performance that high angle of attack maneuvers have a performance payoff only at very low speeds. This occurs because the thrust force dominates the lift at low speed because the dynamic pressure is low. As the speed increases, the aerodynamic lift dominates over the thrust and the maximum turning rates tend to be near α_{stall}. In this section, the impact of both aerodynamic and thrust control will be addressed. The latter includes both thrust magnitude and vector angle variations. It will be assumed throughout that the thrust magnitude does not vary with angle of attack or thrust angle. The equations of motion are Equations (1) through (3)

$$\dot{V} = g(F_T - \sin\gamma) \tag{1}$$

$$\dot{\gamma} = \frac{g}{V}(F_N\cos\sigma - \cos\gamma) \tag{2}$$

$$\dot{\psi} = \frac{g}{V} F_N \frac{\sin\sigma}{\cos\gamma} \tag{3}$$

where F_T and F_N are defined by Equations (4) through (6)

$$F_T = T\cos(\alpha+\delta_v) - D \tag{4}$$

$$F_N = T\sin(\alpha+\delta_v) + L \tag{5}$$

$$T = T/W,\ D = D/W,\ L = L/W \tag{6}$$

The altitude variation will be assumed to be negligible.

The optimal control problem is the minimum time to turn from

$$V(o) = V_o, \ \gamma(o) = 0 \tag{56}$$

to

$$\gamma(t_f) = 0 \tag{57}$$

where V_o is specified. If the motion is in the vertical plane, then the final flight path angle can be taken to be $\pm \pi$. The final speed may be free or it may be specified. If V_o is free, the optimal trajectory is free to go to low speeds if this is optimum. The final heading is free.

There are four controls; the thrust magnitude, the thrust vector angle, the aerodynamic angle of attack, and the bank angle. Optimal controls will be determined for all four. Then the case where the thrust angle is fixed and set equal to zero will be addressed. The contraints on the structural load factor and thrust magnitude, Relations (10) and (11), must hold everywhere along the trajectory. The problem with aerodynamic control at high angles of attack will not be addressed. It will be assumed that there is sufficient control to fly anywhere between zero and ninety degrees.

Nondimensional Transformations

Before developing the optimal controls, it will be useful to introduce nondimensional variables that are the order of one.

Let

$$u = V/V_o, \ \tau = gt/V_o \tag{58}$$

The transformed differential equations are

$$\frac{du}{d\tau} = T' \cos(\alpha+\delta_v) - N' \sin\alpha - \sin\gamma \tag{59}$$

$$\frac{d\gamma}{d\tau} = \frac{1}{u}\left\{\left[T' \sin(\alpha+\delta_v)+N' \cos\alpha\right]\cos\sigma - \cos\gamma\right\} \tag{60}$$

$$\frac{d\psi}{d\tau} = \frac{1}{u}\left[T' \sin(\alpha+\delta_v)+N' \cos\alpha\right] \frac{\sin\sigma}{\cos\gamma} \tag{61}$$

Consider next the development of the optimal controls.

Optimal Controls

The optimal controls are determined from the maximization of the Hamiltonian defined by

$$H = P_u \frac{du}{d\tau} + P_\gamma \frac{d\gamma}{d\tau} + P_\psi \frac{d\psi}{d\tau} \tag{62}$$

where P_u, P_γ, P_ψ are costate variables that must satisfy along the optimal trajectory

$$\frac{dP_u}{d\tau} = -\frac{\partial H}{\partial u} \tag{63}$$

$$\frac{dP_\gamma}{d\tau} = -\frac{\partial H}{\partial \gamma} \tag{64}$$

$$\frac{dP_\psi}{d\tau} = -\frac{\partial H}{\partial \psi} \tag{65}$$

Since H is independent of the heading angle ψ, P_ψ is a constant everywhere along the optimal trajectory. Since the final heading is free

$$P_{\psi} = 0 \tag{66}$$

The boundary condition on the costate variable corresponding to the flight path angle γ is

$$P_{\gamma}(t_f) = P_{\gamma_f} \tag{67}$$

If final speed is free, from the transversality condition

$$P_u(t_f) = 0 \tag{68}$$

If the final speed is prescribed

$$P_u(t_f) = P_{u_f} \tag{69}$$

The optimal angle of attack schedule as a function of time will be different for the free and specified final speed cases. Hereafter we will only consider the case where the final speed is free. The boundary conditions in Equations (66), (67), and (68) must be such that the boundary condition in Equation (57) is satisfied. The final time is free and H does not contain the time, therefore

$$H = C_o \tag{70}$$

everywhere along the optimal trajectory.

Substituting Equations (59) through (61) and (66) into Equation (62) gives

$$H = \lambda_T T + \lambda_N N - P_u \sin\gamma - \frac{P_{\gamma}}{u} \cos\gamma \tag{71}$$

where

$$\lambda_T = P_u \cos(\alpha+\delta_v) + \frac{1}{u} P_\gamma \cos\sigma \sin(\alpha+\delta_v) \tag{72}$$

$$\lambda_N = -P_u \sin\alpha + \frac{1}{u} P_\gamma \cos\sigma \cos\alpha \tag{73}$$

Consider first that part of the Hamiltonian that contains the bank angle

$$H(\sigma) = \frac{1}{u} P_\gamma \cos\sigma [T \sin(\alpha+\delta_v) + N \cos\alpha] \tag{74}$$

There are only two choices that maximize H

$$\sigma^* = 0 \text{ if } P_\gamma > 0 \tag{75}$$

$$\sigma^* = \pi \text{ if } P_\gamma < 0 \tag{76}$$

The final flight path angle is

$$\gamma(t_f) = \pi \text{ if } \sigma^* = 0$$

$$\gamma(t_f) = -\pi \text{ if } \sigma^* = \pi \tag{77}$$

The optimal path is in the vertical plane. If the final speed is free, the optimum is a half loop or split-S both of which are illustrated in Figure 21. If the final speed is specified, then an additional maneuver must be considered. This third maneuver is a pull up to stall, a rotation to a nose down attitude, and then a pull up to zero flight path angle and specified speed. In the numerical examples to be examined later, we will consider only free final speed. The only time that σ^* can be different from 0 or π is when there is an altitude constraint or the final heading

is not π. These possibilities will not be addressed in this effort.

We can now drop Equation (61). Equations (72) and (73) become

$$\lambda_T = P_u \cos(\alpha+\delta_v) + \frac{P_\gamma \delta}{u} \sin(\alpha+\delta_v) \tag{78}$$

$$\lambda_N = -P_u \sin\alpha + \frac{P_\gamma \delta}{u} \cos\alpha \tag{79}$$

where

$$\delta = +1 \quad \text{for a pull up} \tag{80}$$

$$\delta = -1 \quad \text{for a pull down} \tag{81}$$

Consider next optimal thrust magnitude control.

The thrust appears linearly in the Hamiltonian, therefore, for optimal thrust magnitude control

$$T = T_{max} \quad \text{if } \lambda_T > 0 \tag{82}$$

$$T = 0 \quad \text{if } \lambda_T < 0 \tag{83}$$

and may be interior if $\lambda_T = 0$ for a finite time. This situation will be examined later in this section.

Next consider optimization with respect to the thrust vector angle, δ_v. Let $H(\delta_v)$ denote that part of the Hamiltonian that contains δ_v terms

$$H(\delta_v) = \lambda_T T \tag{84}$$

Maximization with respect to δ_v requires that

$$\frac{\partial \lambda_T}{\partial \delta_v} = 0 \tag{85}$$

Substitution of Equation (78) gives

$$-P_u \sin(\alpha+\delta_v) + \frac{P_\gamma \delta}{u} \cos(\alpha+\delta_v) = 0 \tag{86}$$

The solution may be in any quadrant, therefore, the sum is computed from

$$\sin(\alpha+\delta_v) = \pm \frac{P_\gamma \delta}{uP} \quad , \quad \cos(\alpha+\delta_v) = \pm \frac{P_u}{P} \tag{87}$$

where

$$P = \left[P_u^2 + \left(\frac{P_\gamma}{u} \right)^2 \right]^{1/2} \tag{88}$$

Substitution of Equations (87) into Equation (78) gives

$$\lambda_T = \pm P \tag{89}$$

Maximum $H(\delta_v)$ corresponds to maximum λ_T, therefore, the positive sign holds and

$$\lambda_T = P \tag{90}$$

$$H(\delta_v) = PT \tag{91}$$

$$\sin(\alpha+\delta_v) = \frac{P_\gamma \delta}{uP} \quad , \quad \cos(\alpha+\delta_v) = \frac{P_u}{P} \tag{92}$$

Intermediate thrust can be ruled out since this would require P to be zero which requires P_u and P_γ both to be zero according to Equation (88). This can not hold for a trajectory optimization problem, the costate variables cannot all be zero. Thus, maximum thrust magnitude is applied throughout the trajectory.

The optimal angle of attack is determined next. Let $H(\alpha)$ denote that part of the Hamiltonian that contains α terms

$$H(\alpha) = \lambda_T T + \lambda_N N \tag{93}$$

The necessary condition for optimum α is

$$\frac{\partial H(\alpha)}{\partial \alpha} = \frac{\partial \lambda_T}{\partial \alpha} T + \frac{\partial \lambda_N}{\partial \alpha} N + \lambda_N \frac{\partial N}{\partial \alpha} = 0 \tag{94}$$

Since

$$\frac{\partial \lambda_T}{\partial \alpha} = \frac{\partial \lambda_T}{\partial \delta_v} = 0 \tag{95}$$

Equation (94) becomes

$$\left(-P_u \cos\alpha - \frac{P_\gamma \delta}{u} \sin\alpha\right) N + \left(-P_u \sin\alpha + \frac{P_\gamma \delta}{u} \cos\alpha\right) N_\alpha = 0 \tag{96}$$

This is a transcendental equation in α. Solving for $\tan\alpha$ gives

$$\tan\alpha = \frac{\frac{C_{N_\alpha}}{C_N} - \frac{uP_u}{P_\gamma \delta}}{1 + \frac{C_{N_\alpha}}{C_N}\frac{uP_u}{P_\gamma \delta}} \tag{97}$$

This equation can be solved for the costate function

$$P_R = \frac{uP_u}{P_\gamma \delta} \tag{98}$$

as a function of the optimal angle of attack. Figure 22 presents the optimal angle of attack as a function of the costate function P_R. If the final speed is free, then the final value of P_R is zero. Equation (97) reduces to

$$\tan\alpha = \frac{C_{N_\alpha}}{C_N} \tag{99}$$

Differentiating Equation (21) gives

$$C_{L_\alpha} = C_{N_\alpha}\cos\alpha - C_N \sin\alpha \tag{100}$$

Substituting Equation (99) gives $C_{L_\alpha} = 0$. Thus, at the final time the optimal angle of attack is the stall angle. Also at the final time, Equation (92) gives

$$\alpha + \delta_v = \frac{\pi}{2} \tag{101}$$

Recall for the instantaneous turning problem the optimum angle of attack was α_{stall} and the thrust vector angle was the complement

of α_{stall} which is the same as the final condition for the problem here.

From Equations (92)

$$\cot\varepsilon^{\star} = P_R \tag{102}$$

where

$$\varepsilon^{\star} = \alpha^{\star}+\delta_v^{\star} \tag{103}$$

Substituting this into Equation (97) results in a relation between $\varepsilon^{\star}$ and $\alpha^{\star}$ that must be satisfied everywhere along the optimal trajectory

$$\cot\varepsilon = \frac{\frac{C_{N_\alpha}}{C_N} - \tan\alpha}{1 + \frac{C_{N_\alpha}}{C_N}\tan\alpha} \tag{104}$$

The relationship between the optimal angle of attack and optimal epsilon is presented in Figure 23. Given the optimal angle of attack, the optimal thrust vector angle can be determined. The distribution is presented in Figure 24. At high angles of attack where $C_{N_\alpha} = 0$, Equation (104) reduces to

$$\cot\varepsilon = -\tan\alpha \tag{105}$$

The solution of this equation is

$$\varepsilon^{\star} = \frac{\pi}{2} + \alpha^{\star} \tag{106}$$

The solution for optimal δ_v is therefore

$$\delta_v^* = \frac{\pi}{2} \tag{107}$$

This holds whenever $C_{N_\alpha} = 0$. For small angles of attack, C_N is approximately $C_{N_\alpha} \alpha$. Equation (104) is approximately

$$\varepsilon^* = 2\alpha^* \tag{108}$$

The optimal thrust vector angle at low angles of attack is approximately

$$\delta_v^* = \alpha^* \tag{109}$$

For free final speed, the final optimal angle of attack is the stall angle of attack. The only way that higher angles of attack can be reached is if the costate function P_R is less than zero. This can be seen from examination of Equation (97) or Figure 22.

In addition to satisfying Equation (96), it is necessary for a relative maximum that $H(\alpha)$ satisfy

$$\frac{\partial^2 H(\alpha)}{\partial \alpha^2} < 0 \tag{110}$$

Substitution gives

$$\frac{\partial^2 H(\alpha)}{\partial \alpha^2} = -\lambda_T T' - \lambda_N N' + 2 \frac{\partial \lambda_N}{\partial \lambda} \frac{\partial N'}{\partial \alpha} + \lambda_N \frac{\partial^2 N}{\partial \alpha} \tag{111}$$

Since $\lambda_T > 0$, it follows that $\lambda_N > 0$. Also, $N_\alpha \geq 0$, $N'_{\alpha\alpha} \leq 0$, $T' > 0$, $N' > 0$ thus substitution does verify that Relation (110) is satisfied.

Since the optimal maneuvers are in the vertical plane, the trajectories are either a half-loop or a split-S. For a half-loop, $\sigma = 0$, $\delta = 1$, and $\gamma(t_f) = \pi$. For a split-S, $\sigma = \pi$, $\delta = -1$, and $\gamma(t_f) = -\pi$. These terminal conditions replace Equation (57). The optimal trajectory is the maneuver that gives the minimum time to rotate through 180 degrees in the flight path angle. This can only be determined by numerically integrating the appropriate differential equations and comparing times for a half-loop and a split-S.

The differential equations that must be solved simultaneously are the differential equations for u, γ, P_u, and P_γ. Since the optimal controls are a function of P_R, the differential equations for P_u and P_γ can be replaced with a single differential equation for P_R. Differentiating the logarithm of P_R gives.

$$\frac{dP_R}{d\tau} = \frac{P_R}{u}\frac{du}{d\tau} + \frac{P_R}{P_u}\frac{dP_u}{d\tau} - \frac{P_R}{P_\gamma}\frac{dP_\gamma}{d\tau} \qquad (112)$$

Substituting Equation (59) for $du/d\tau$ and expanding Equations (63) and (64) for $dP_u/d\tau$ and $dP_\gamma/d\tau$ gives after some manipulation

$$\frac{dP_R}{d\tau} = \frac{1}{u}T'(P_R\cos\varepsilon+\sin\varepsilon) + \frac{1}{u}N'(P_R\sin\alpha-\cos\alpha) - \frac{1}{U}\delta(1+P_R^2)\cos\gamma \qquad (113)$$

Substituting Equations (92) for ε gives

$$\frac{dP_R}{d\tau} = \frac{1}{u} T (1+P_R^2)^{1/2} + \frac{1}{u} N (P_R \sin\alpha - \cos\alpha) - \frac{1}{u} \delta(1+P_R^2)\cos\gamma \quad (114)$$

The right side is a function of the costate variable P_R, the state variables u and γ, and the control variables T and α. The differential equations for u and γ are a function of the state and control variables. The control variable α is a function of the costate variable and the thrust is maximum. Thus, three differential equations result, one each for P_R, u, and γ. The only unknown is the initial value for P_R. But the final value is known from Equation (68). Thus, a single parameter search on the initial value of P_R is required. An initial estimate is made, the three differential equations are integrated forward in time, and the optimal trajectory is that trajectory that gives $P_R(\tau_f) = 0$. Later on in this section, we will develop some numerical results. Consider next the problem where the thrust vector angle is fixed at zero.

Zero Thrust Vector Angle

Equations (92) do not apply. Equation (94) for optimal α becomes upon substitution of Equations (78) and (79) with $\delta_v = 0$

$$\frac{\partial H(\alpha)}{\partial \alpha} = \lambda_N T - \lambda_T N + \lambda_N \frac{\partial N}{\partial \alpha} = 0 \quad (115)$$

This equation is different from Equation (94) because of the $\lambda_N T$ term. Equation (110) becomes

$$\frac{\partial^2 H(\alpha)}{\partial \alpha^2} = -\lambda_T T - \lambda_N N - 2\lambda_T \frac{\partial N}{\partial \alpha} + \lambda_N \frac{\partial^2 N}{\partial \alpha^2} < 0 \quad (116)$$

Solving Equation (115) for λ_N and substituting gives

$$\frac{\partial^2 H(\alpha)}{\partial \alpha^2} = -\lambda_T \left[T + 2 \frac{\partial N}{\partial \alpha} + \left(N - \frac{\partial^2 N}{\partial \alpha^2} \right) \frac{N}{T + \frac{\partial N}{\partial \alpha}} \right] \tag{117}$$

Since the first derivative of N is non negative and the second derivative is non positive, the bracket sum is non negative and it follows that if Relation (117) is satisfied, then

$$\lambda_T > 0 \tag{118}$$

The thrust magnitude is maximum except for possible interior thrust. Consider this possibility. For interior thrust, $\lambda_T = 0$ for a finite time, thus Equation (115) reduces to

$$\frac{\partial H(\alpha)}{\partial \alpha} = \lambda_N \left(T + \frac{\partial N}{\partial \alpha} \right) = 0 \tag{119}$$

The only possibility is

$$\lambda_N = 0 \tag{120}$$

If both λ_N and λ_T are zero, then Equations (78) and (79) reduce to

$$P_u \cos\alpha + \frac{P_\gamma \delta}{u} \sin\alpha = 0 \tag{121}$$

$$\frac{P_\gamma \delta}{u} \cos\alpha - P_u \sin\alpha = 0 \tag{122}$$

These two equations combined together give

$$P_u^2 + \left(\frac{P_\gamma}{u}\right)^2 = 0 \qquad (123)$$

This can hold if and only if

$$P_u = P_\gamma = 0 \qquad (124)$$

This can not hold for the optimal solution. Therefore $\lambda_T \neq 0$ for a finite time and maximum thrust is applied everywhere along the optimal trajectory.

The optimal angle of attack is the solution of Equation (115). Substituting Equations (78) and (79) gives

$$(-P_u \sin\alpha + \frac{P_\gamma \delta}{u} \cos\alpha)(T + N_\alpha) - (P_u \cos\alpha + \frac{P_\gamma \delta}{u} \sin\alpha)N = 0 \qquad (125)$$

Since the optimal angle of attack is between zero and ninety degrees, Equation (125) can be rewritten as

$$\tan\alpha = \frac{T + N_\alpha - P_R N}{P_R(T + N_\alpha) + N} \qquad (126)$$

The optimal angle of attack is the solution of Equation (126).

At the final time, $P_u = 0$ from Equation (64). Substitution into Equation (126) gives

$$\tan\alpha = \frac{T + N_\alpha}{N} \qquad (127)$$

Comparison with Equation (26) shows that the final value of the optimal angle of attack is equal to the optimal instantaneous value. Thus, if the final speed is higher than the critical

speed, the final angle of attack is close to α_{stall}. The only time that high angle of attack could occur is at speeds less than the critical speed. In air combat, this situation is to be avoided since the engangement is similar to that between helicopters and fighters. But from strictly a single vehicle minimum time turn problem, the angle of attack could attain large values if the speed is very low.

Numerical Examples

Optimal controls for zero thrust vectoring will not be emphasized since it was shown in the last section that high angle of attack maneuvers can result. With thrust vectoring there is uncertainty as to whether or not PSM is optimal. At this point all that we know is that the final value of the optimal angle of attack equals the stall value.

Optimal and nominal trajectories were developed for initial conditions corresponding to 0.6 Mach Number and 20,000 feet altitude. The nominal trajectories correspond to constant angle of attack and thrust vector angle. The angle of attack was α_{stall}. Optimal trajectories were in the vertical plane. The pull up maneuver required less time to rotate through 180 degrees than did a split-S maneuver.

The numerical results are presented in Table 1. Six different cases are presented. The thrust to weight ratio of 0.6 is a typical value for the F15 at 20,000 feet and 0.6 Mach Number. Higher values of T' were introduced to determine the effect of increasing thrust. The first two cases were nominal trajectories flown at $C_{L_{max}}$, i.e., α_{stall}. The difference was in the thrust vector angle. Thrust vectoring reduced the time by approximately three and one half seconds. The last four cases are optimal results. The third and fourth cases show the difference between a pull up and a split-S maneuver. The pull up is better.

Comparison of the third, fifth, and last case shows that the time decreases as the thrust to weight increases. This is consistent with the results from the previous section. There the turning rate increased with increasing thrust to weight ratio. The angle of attack did reach values where $C_N = C_{N_{max}}$. The thrust vector angle went to ninety degrees.

TABLE 1

TIME TO TURN RESULTS

T/W	MANEUVER	MAX α (Deg)	MAX δ_v (Deg)	TIME (SEC)
0.6	PULL UP	α_{stall}	$90-\alpha_{stall}$	10.8
0.6	PULL UP	α_{stall}	0	14.5
0.6	PULL UP	50	90	9.6
0.6	SPLIT-S	30	60	12.3
1.0	PULL UP	55	90	7.9
1.2	PULL UP	60	90	7.3

Based upon the limited number of numerical results examined here, the conclusion is that for minimum time turns, post stall maneuvering is optimal. This holds for both thrust vectoring and nonvectoring.

In Figures 25 through 29, u, γ, P_R, α, and δ_v are presented as a function of the nondimensional time and for initial values of P_R equal to 0.3, 0.4, 0.5, 0.6, and 0.7. These results correspond to the third case in Table 1. The trajectories for P_R (0) = 0.3 and 0.4 do not generate enough lift to fly through the vertical, thus the heading can not change by 180 degrees. The optimal trajectory corresponds approximately to P_R (0) = 0.5. In Figure 28 it can be seen that the maximum angle of attack is approximately 50 degrees. From Figure 25 it can be observed that

the final speed is very low. These results demonstrate that high angle of attack maneuvers are optimal with thrust vectoring.

Summary

Minimum time turns in the subsonic region require maximum thrust throughout the maneuver. This holds for both vectored and nonvectored thrust. For the vectored thrust case the final angle of attack equals α_{stall} which matches the instantaneous problem which holds everywhere. For nonvectored thrust the final angle of attack equals that for maximum instantaneous turning rate. Optimal maneuvers employ PSM. As the thrust to weight ratio increases so does the maximum angle of attack along the trajectory.

SECTION V

CONCLUSIONS

The purpose of this effort was to determine whether or not there are any apparent performance improvements through Post Stall Maneuvers (PSM) or thrust vectoring. PSM is a result of high angles of attack, greater than the stall value. Two different problems were addressed. The first examined instantaneous turning performance. The second focused on minimum time turn problems. The impact of both vectored and nonvectored thrust was considered. It was proven that minimum time turns fall in the vertical plane.

For maximum instantaneous turning rate and nonvectored thrust high angle of attack results if the speed is less than the critical speed which is approximately Mach 0.2. The optimal angle of attack approaches ninety degrees as the speed approaches zero. For vectored thrust, the stall angle of attack is optimum and the thrust vector angle is the complement of the angle of attack. PSM is not optimal if thrust vectoring is available.

For minimum time turning performance, maximum thrust is optimal. At the end of the trajectory, the optimal angle of attack equals that for maximum instantaneous performance. PSM is optimal. As the thrust to weight ratio increases, the maximum angle of attack increases.

Future studies should address the following aspects:

1. Unsteady aerodynamics

2. Analysis of aircraft pointing

3. Compare turning versus pointing

4. Air combat analysis MvN

REFERENCES

1. Hedrick, J.K. and Bryson, A.E., "Minimum Time Turns for a Supersonic Airplane at Constant Altitude," Journal of Aircraft, Vol 8, No. 3, March 1971, pp 182-187.

2. Hedrick, J.K. and Bryson, A.E., "Three-Dimensional, Minimum-Time Turns for a Supersonic Aircraft," Journal of Aircraft, Vol 9, No. 2, Feb 1972, pp 115-121.

3. Shinar, J., Marari, A., Blank, D., and Medinah, E.M., "Analysis of Optimal Turning Maneuvers in the Vertical Plan," AIAA Paper 78-1333, Palo Alto, Aug 1978.

4. Vinh, N.X., "Optimal Trajectories in Atmospheric Flight," Elsevier, Amsterdam-Oxford-New York, 1981.

5. Lin, C.F., "Optimum Maneuvers of Supersonic Aircraft," PhD Dissertation, University of Michigan, 1980.

6. Givan, M.E. and Glass, K.J., "Analysis of Wind Tunnel Data Pertaining to Aerodynamics of Fighter Configurations at High Angle-of-Attack," AFFDL-TR-78-187, January 1979, McDonnell Aircraft Company.

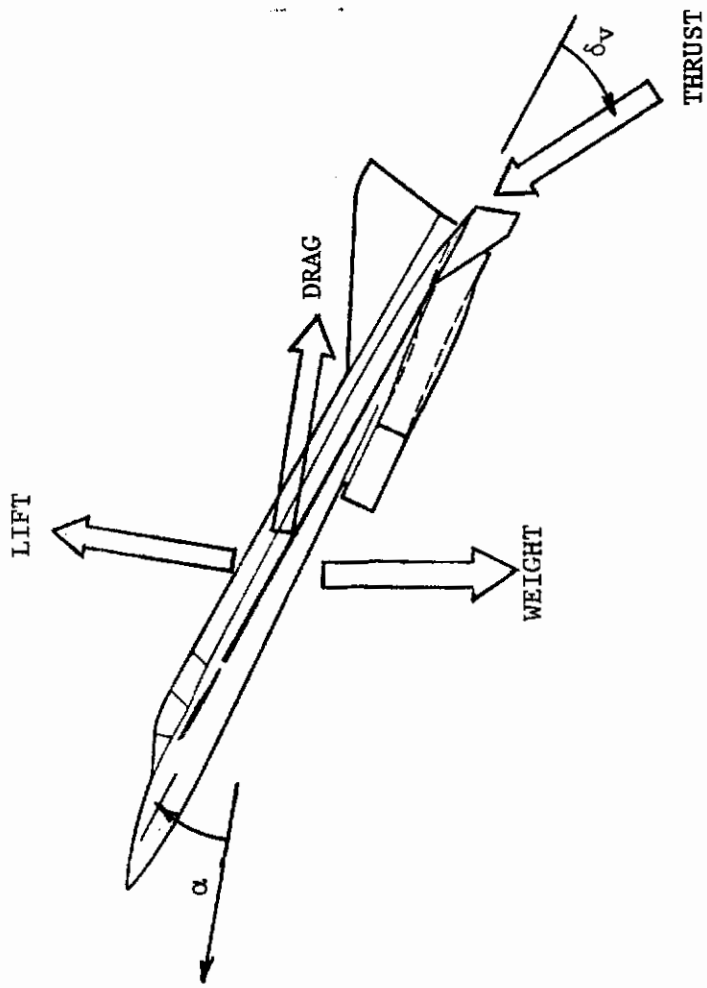

FIGURE 1. Weight, Aerodynamic, and Propulsive Forces

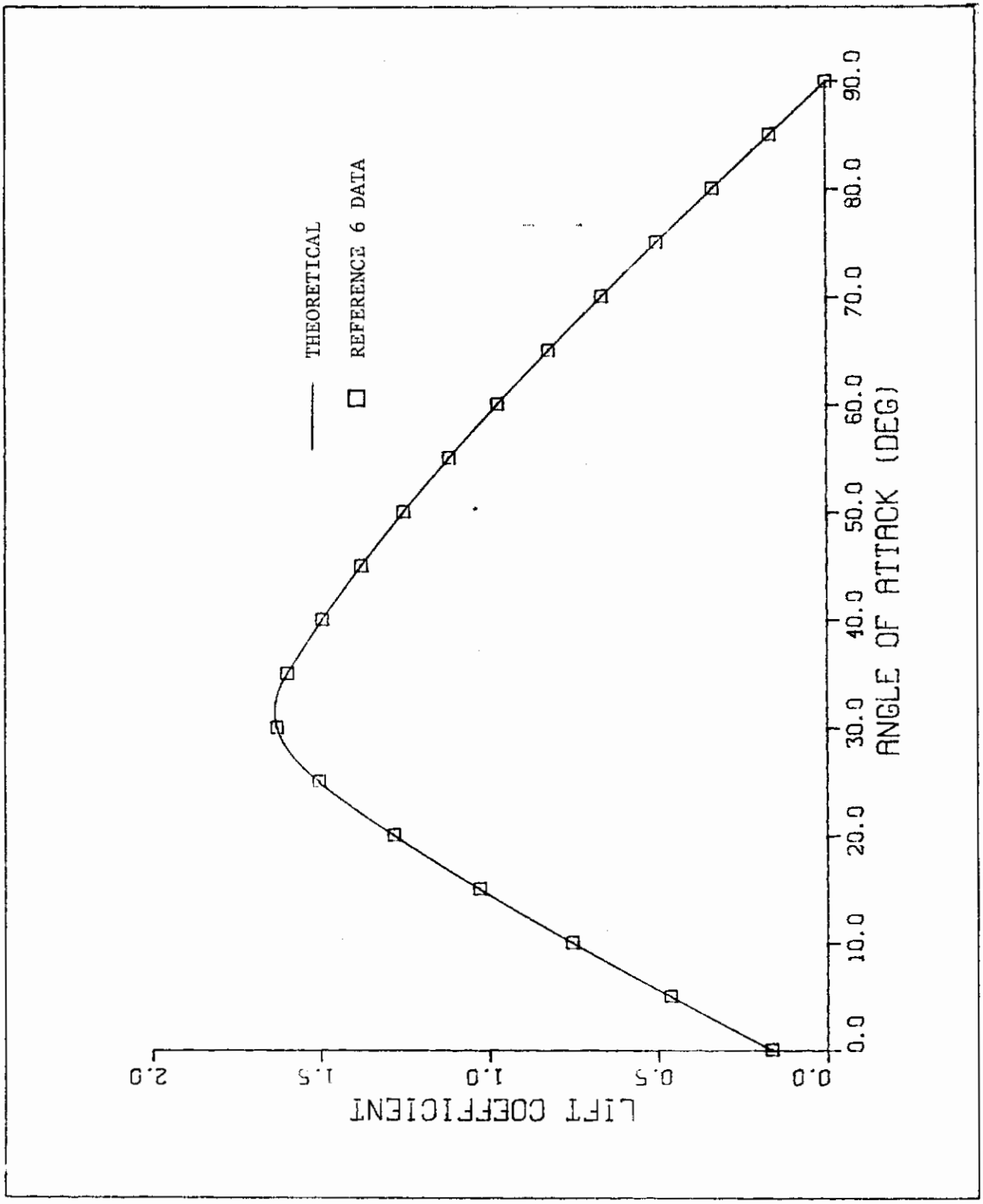

FIGURE 2. F15 Aerodynamic Lift Coefficient

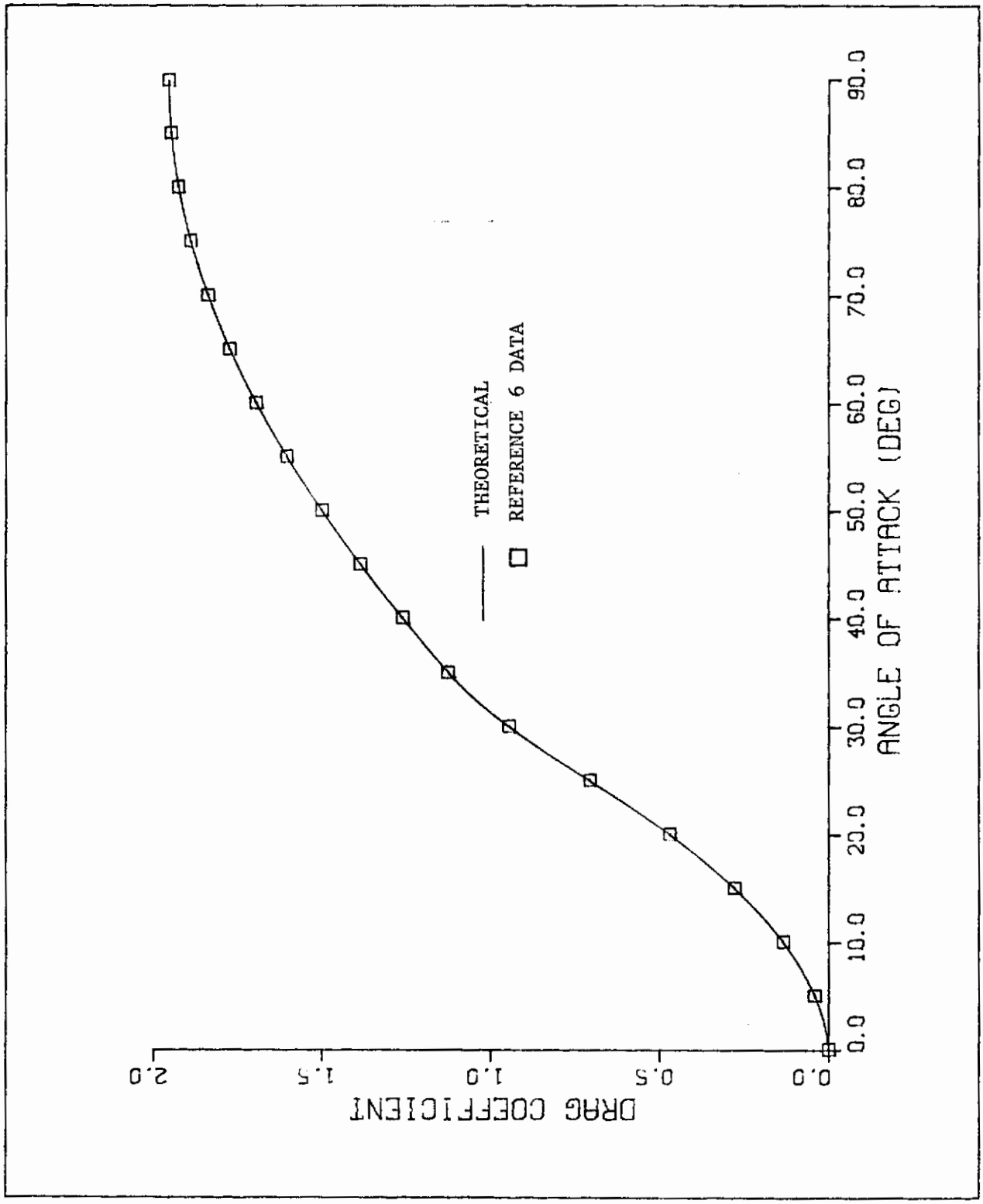

FIGURE 3. F15 Aerodynamic Drag Coefficient

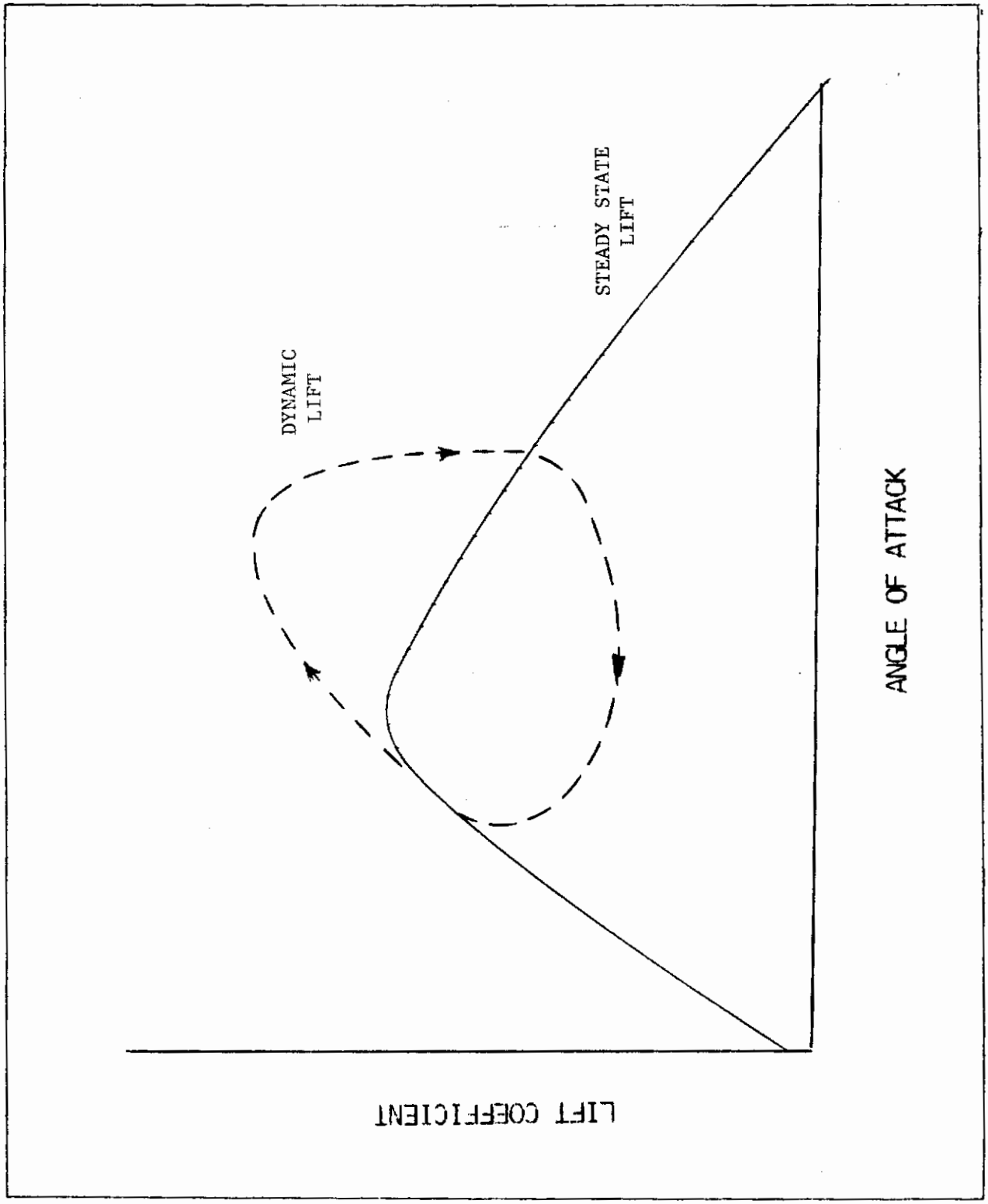

FIGURE 4. Steady State and Dynamic Lift

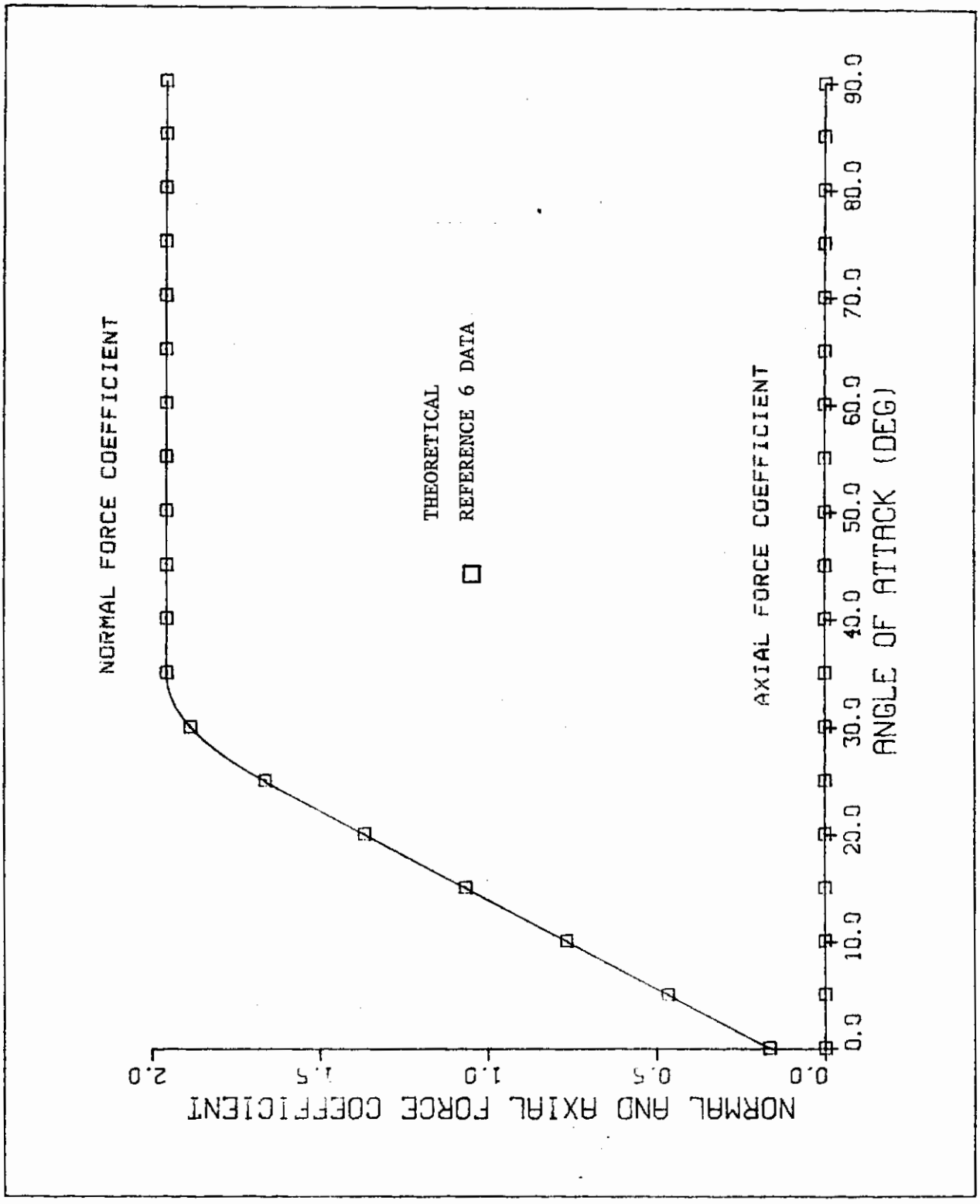

FIGURE 5. F15 Aerodynamic Normal and Axial Force Coefficients

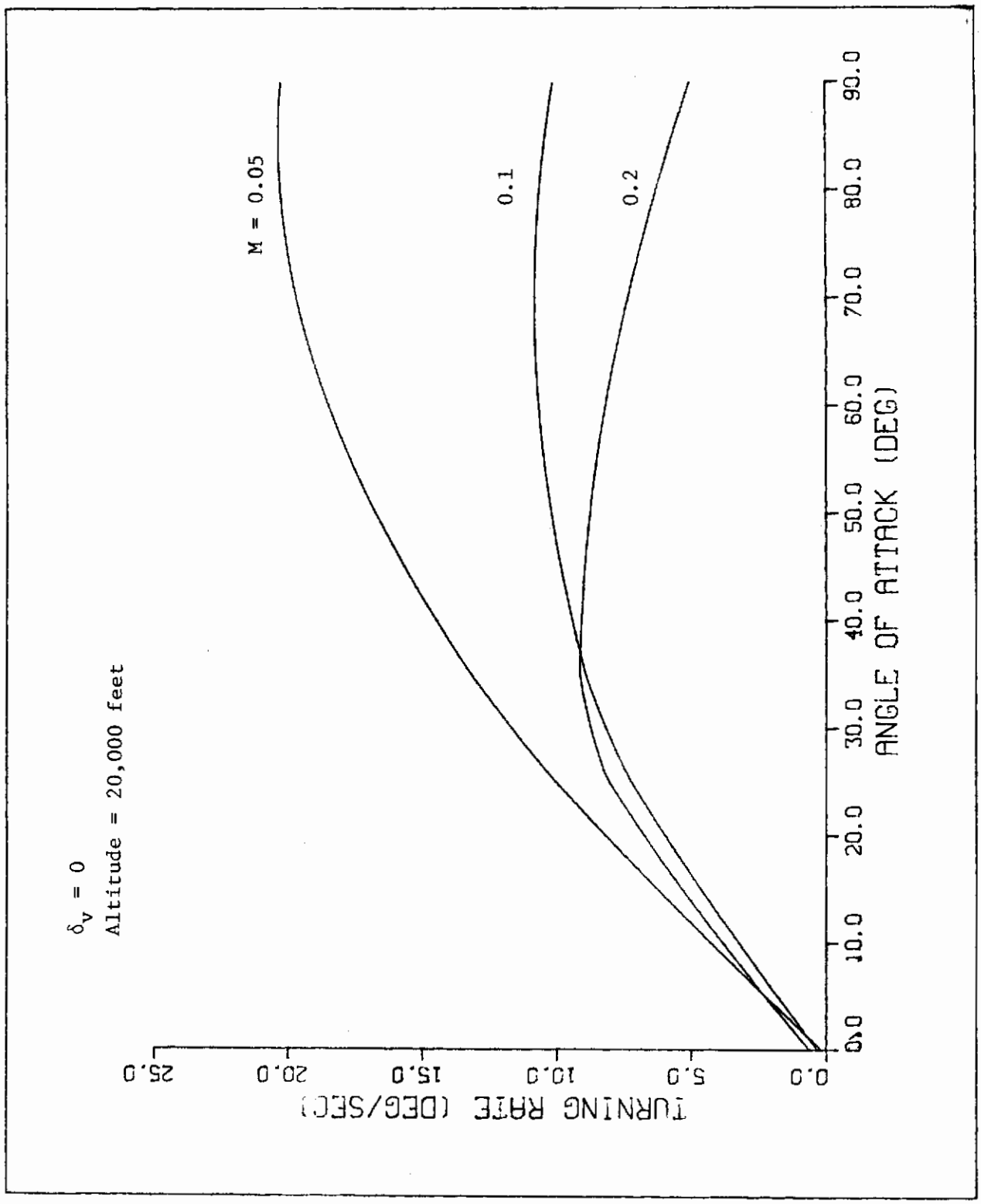

FIGURE 6. Turning Rate as a Function of Angle of Attack and Mach Number Variations

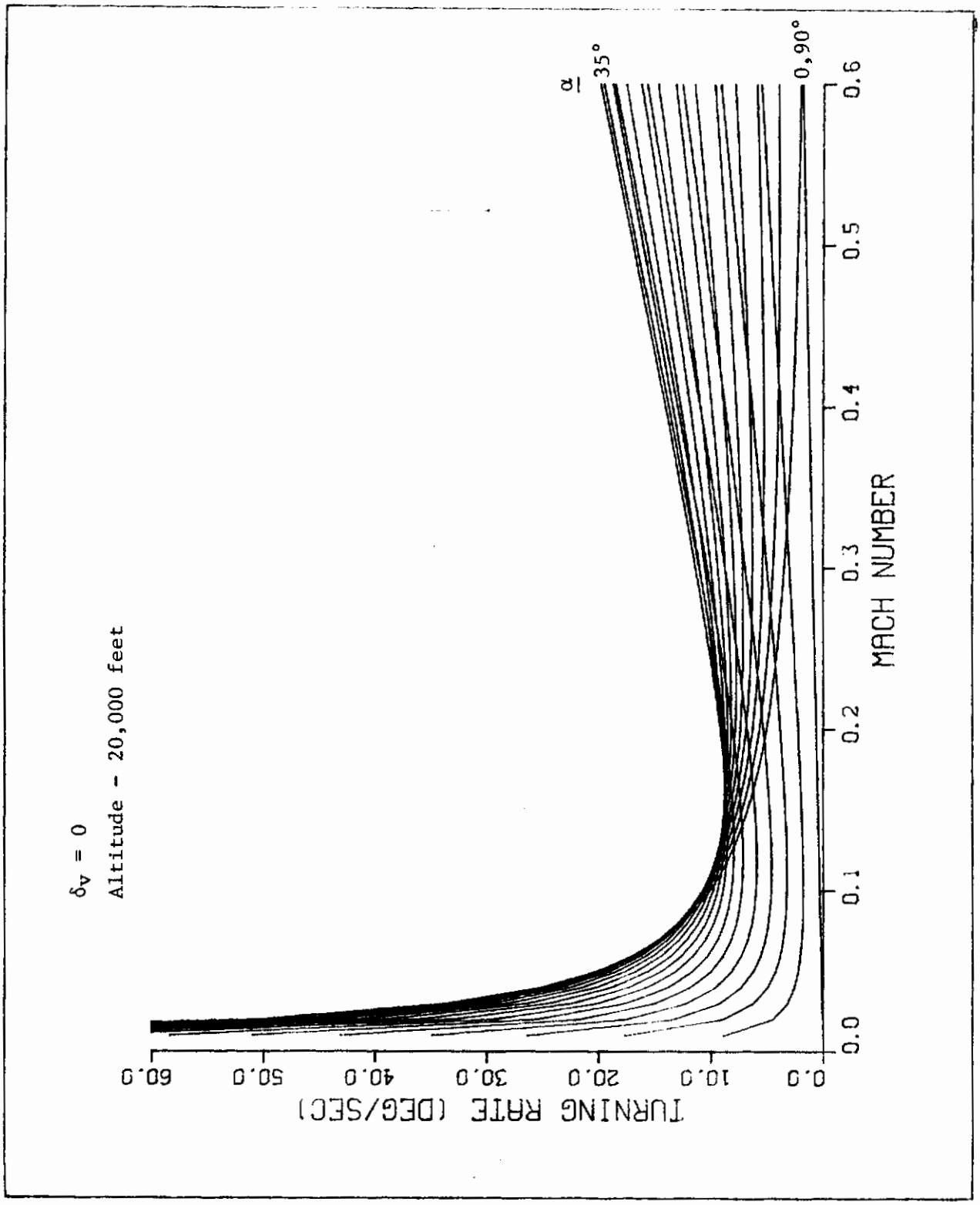

FIGURE 7. Turning Rate as a Function of Angle of Attack and Mach Number

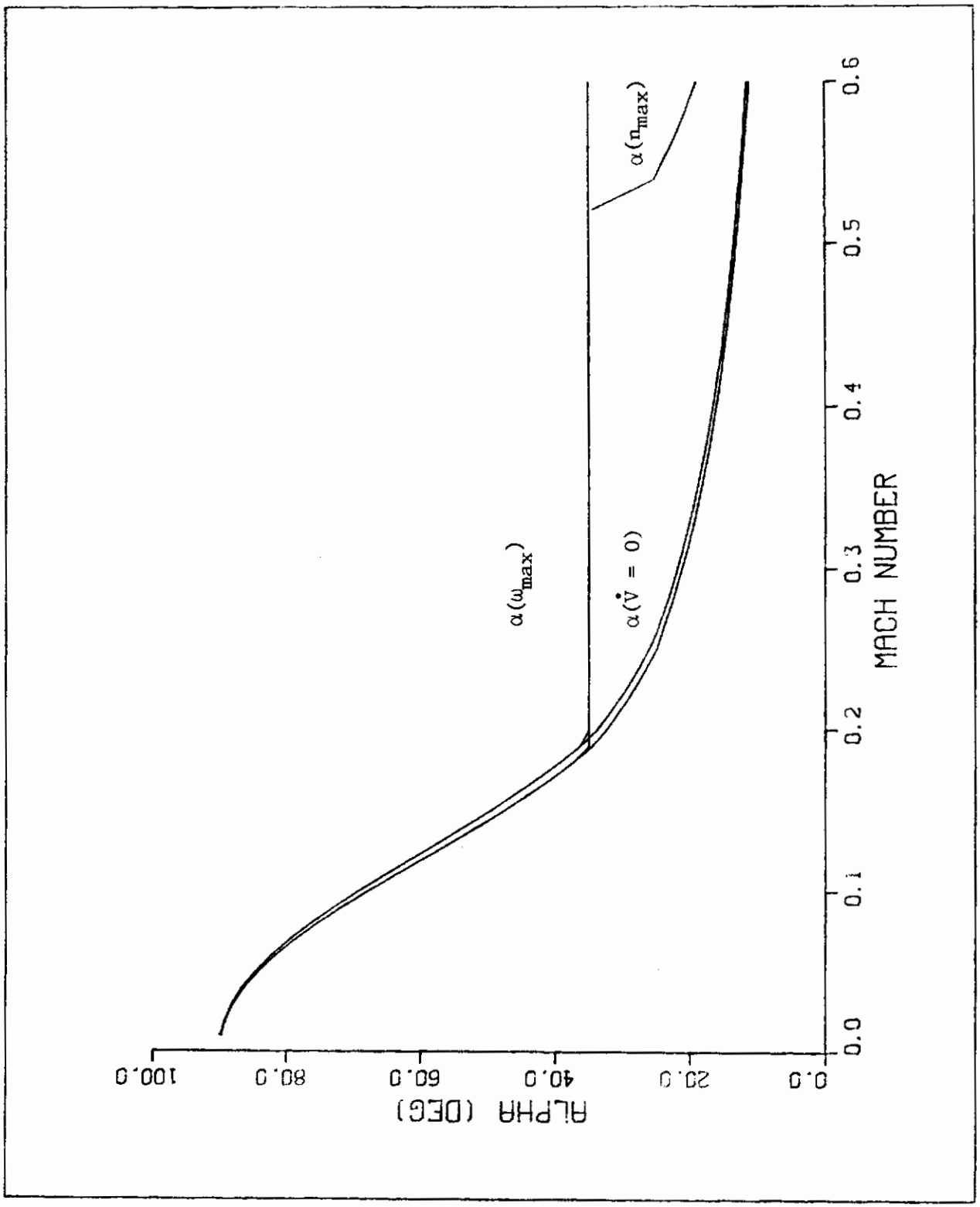

FIGURE 8. Angle of Attack as a Function of Controls and Mach Number

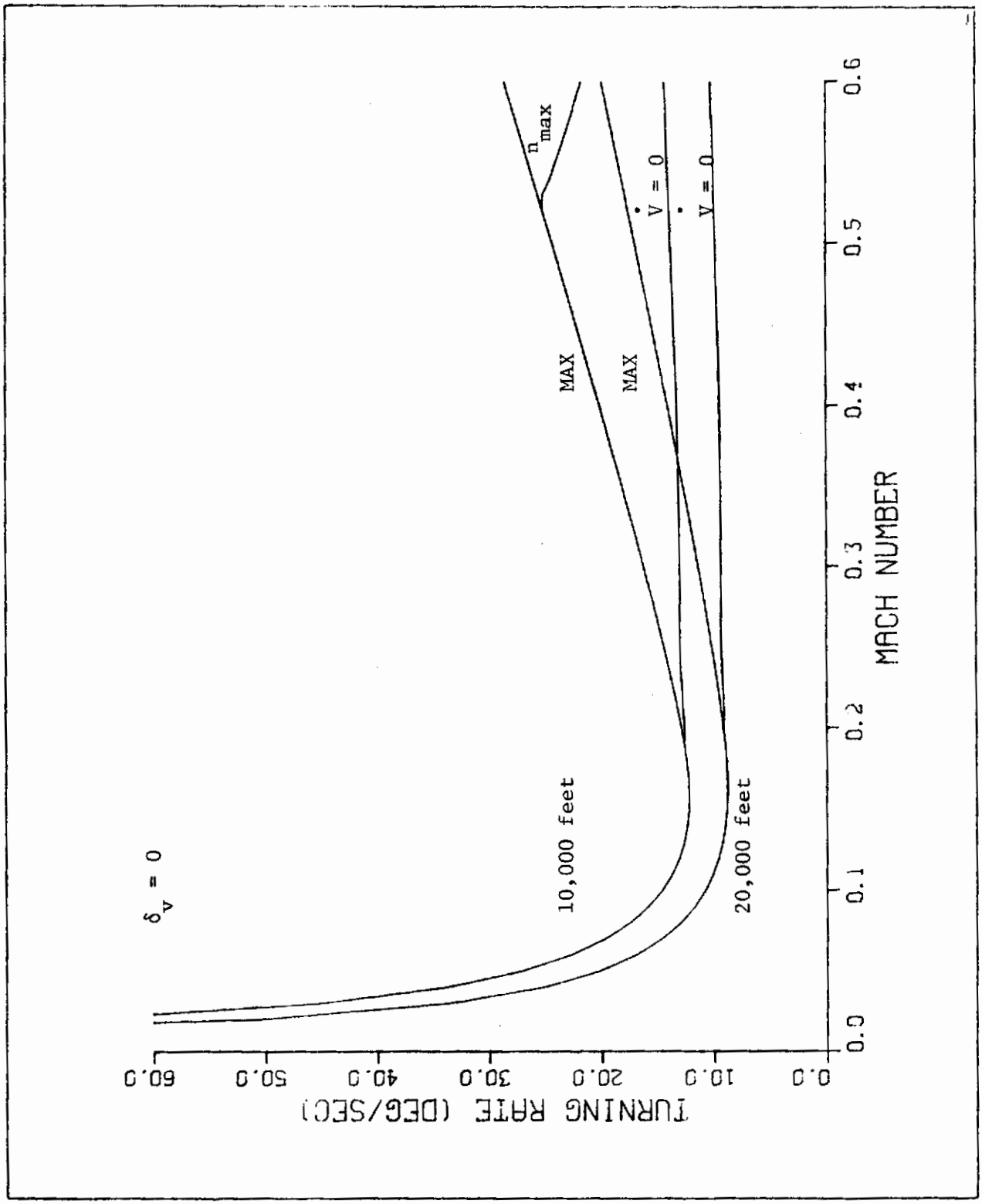

FIGURE 9. Turning Rate as a Function of Controls, Altitude, and Mach Number

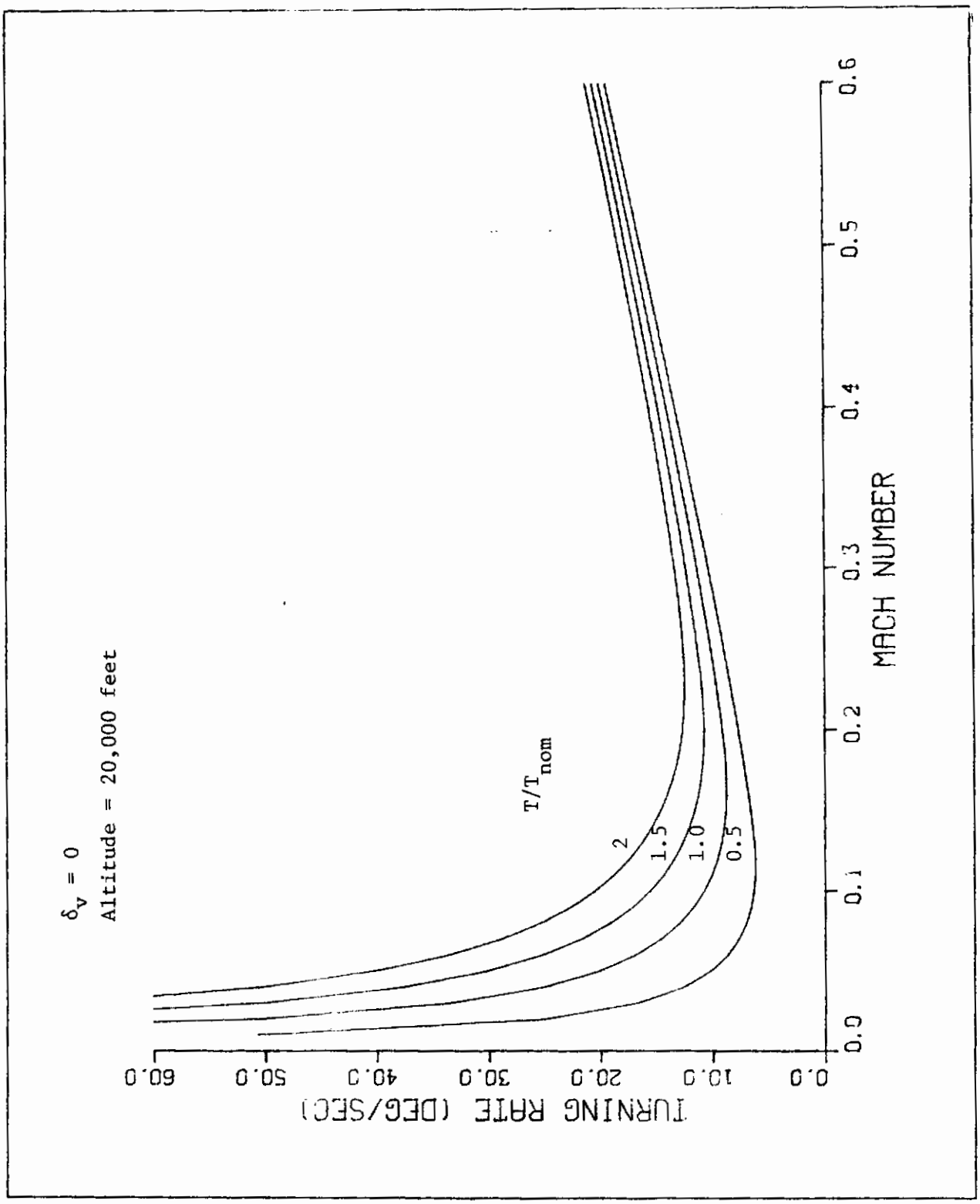

FIGURE 10. Maximum Turning Rate as a Function of Thrust Variations

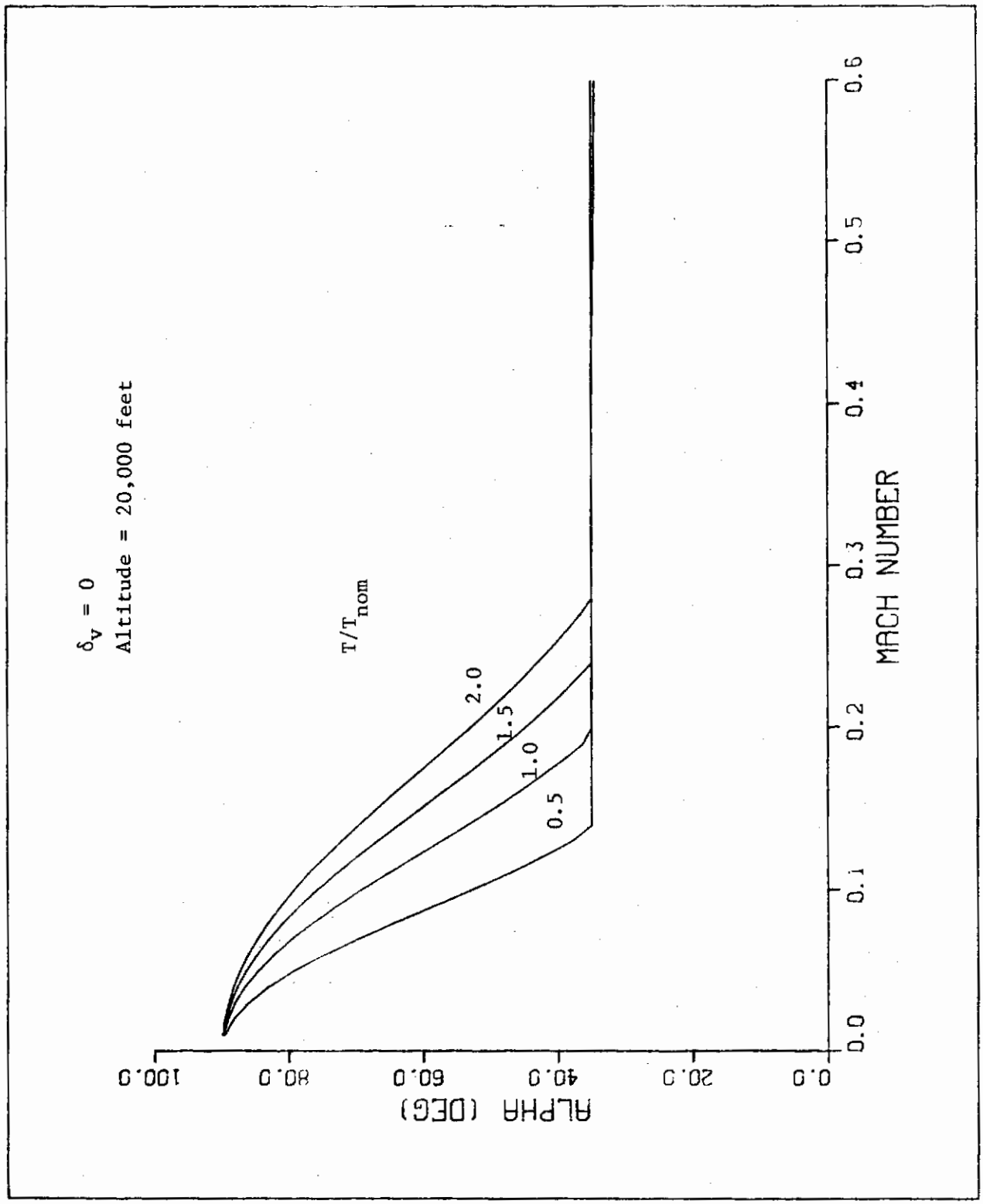

FIGURE 11. Optimum Angle of Attack as a Function of Thrust Variations

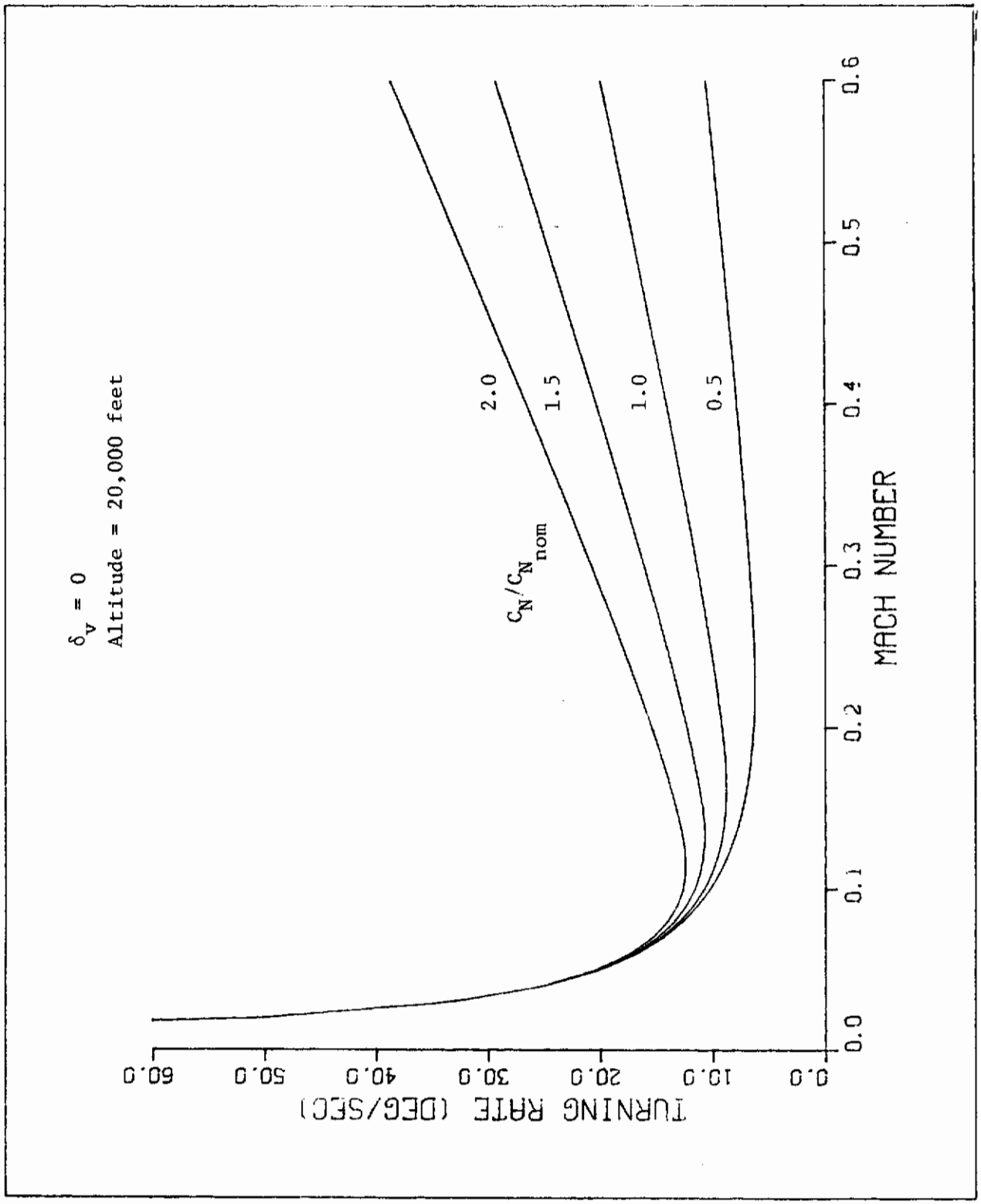

FIGURE 12. Maximum Turning Rate as a Function of Aerodynamic Variations

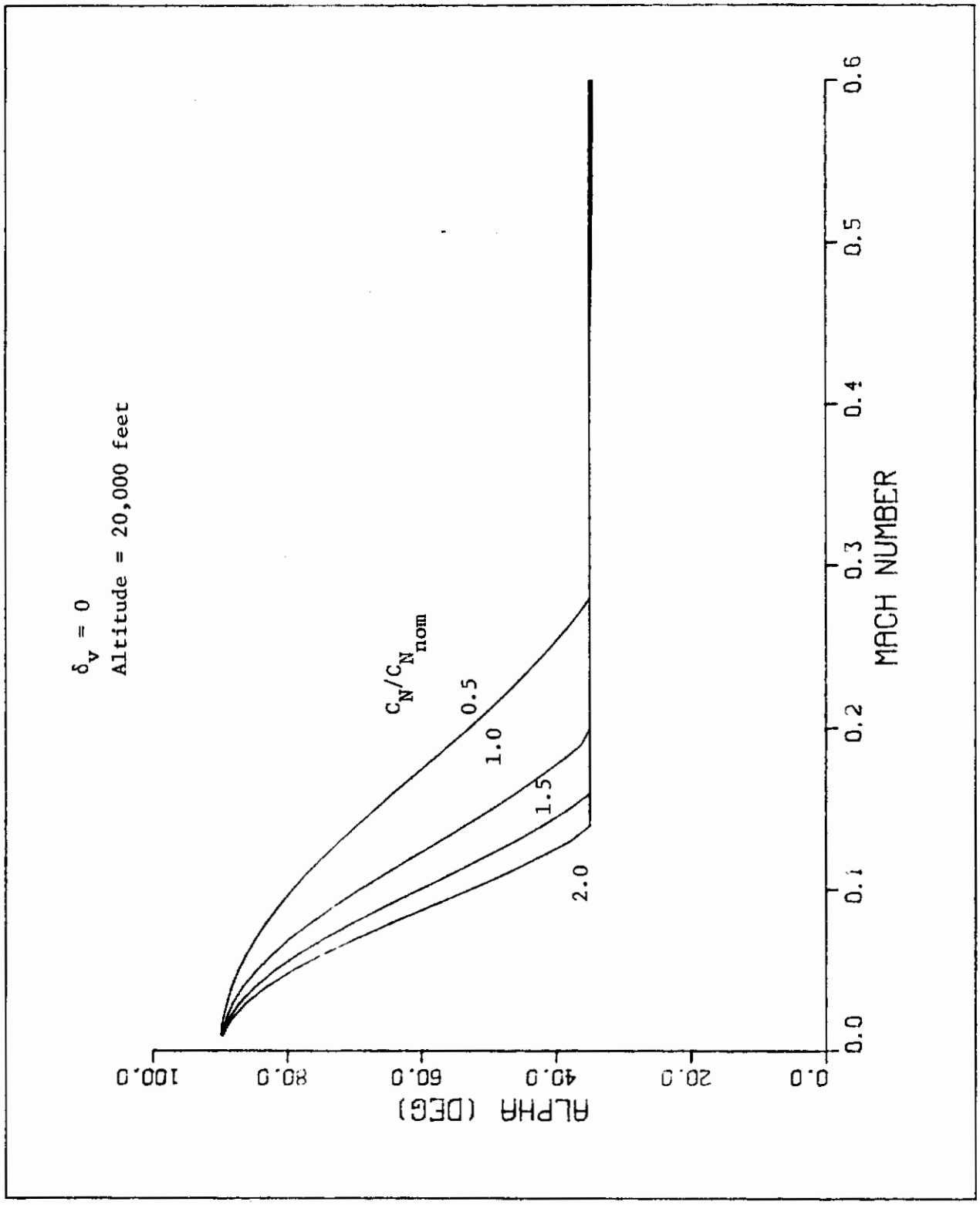

FIGURE 13. Optimum Angle of Attack as a Function of Aerodynamic Variations

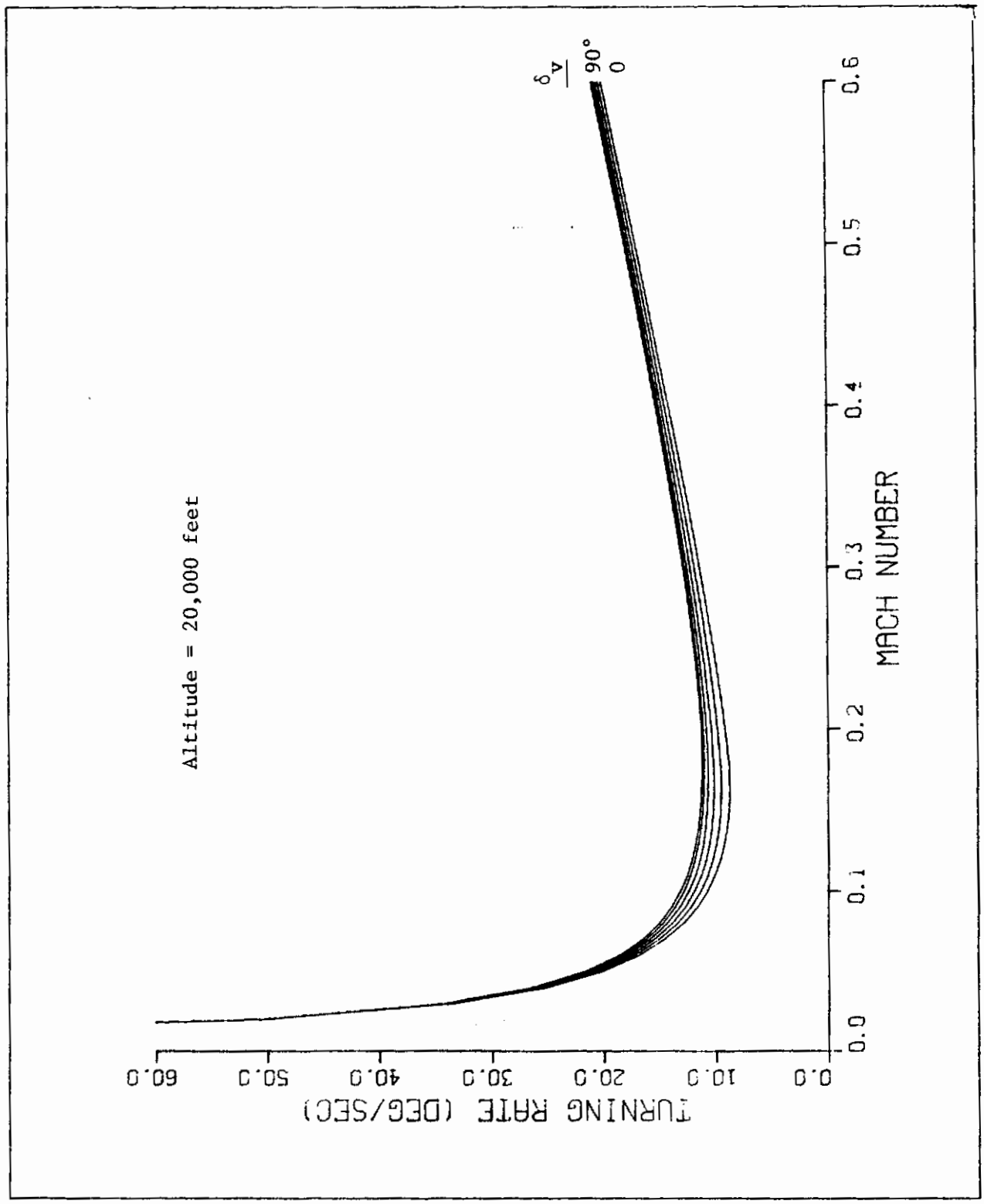

FIGURE 14. Maximum Turning Rate as a Function of Thrust Vector Angle

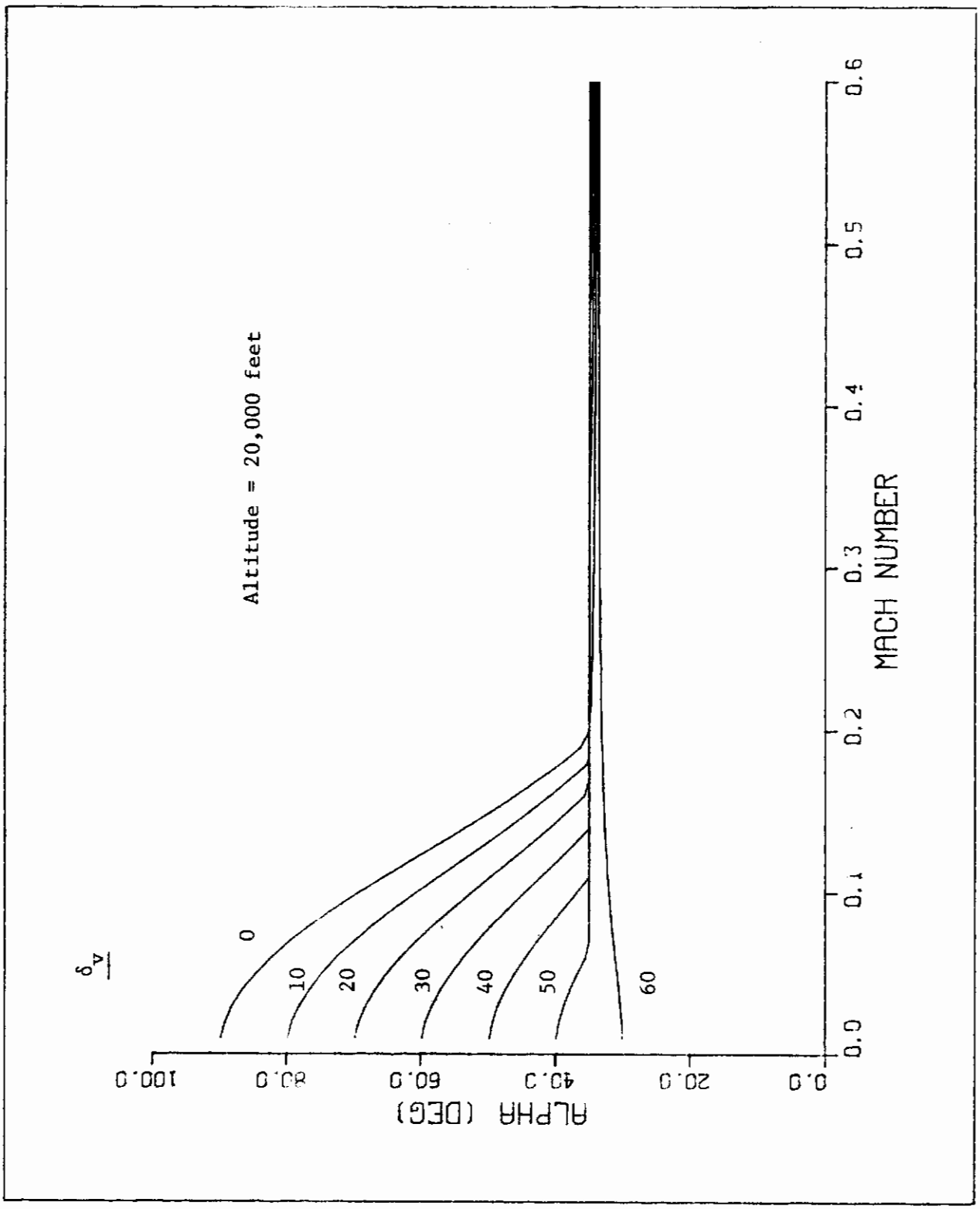

FIGURE 15. Angle of Attack for Maximum Turning Rate as a Function of Thrust Vector Angle

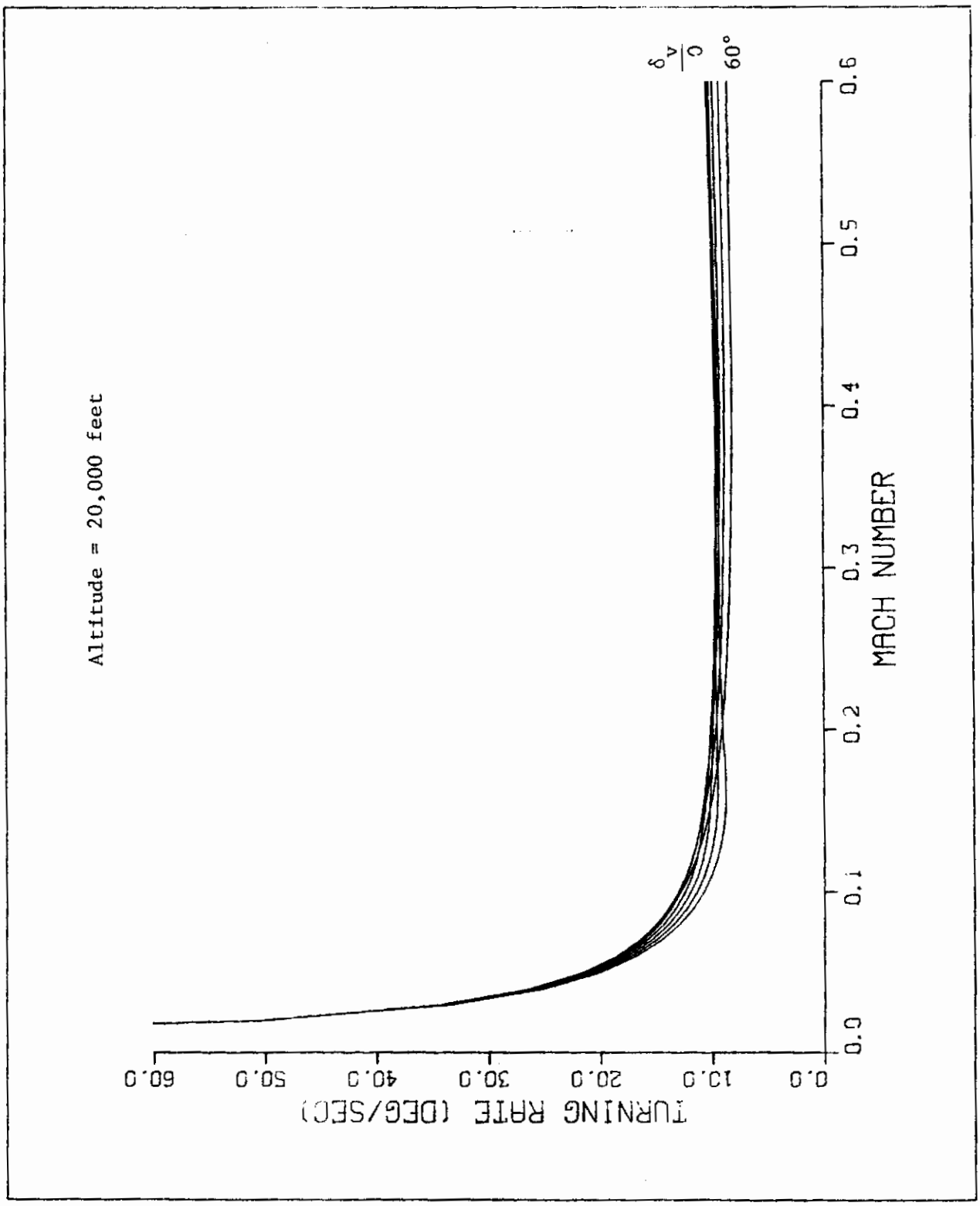

FIGURE 16. Sustained Turning Rate as a Function of Thrust Vector Angle

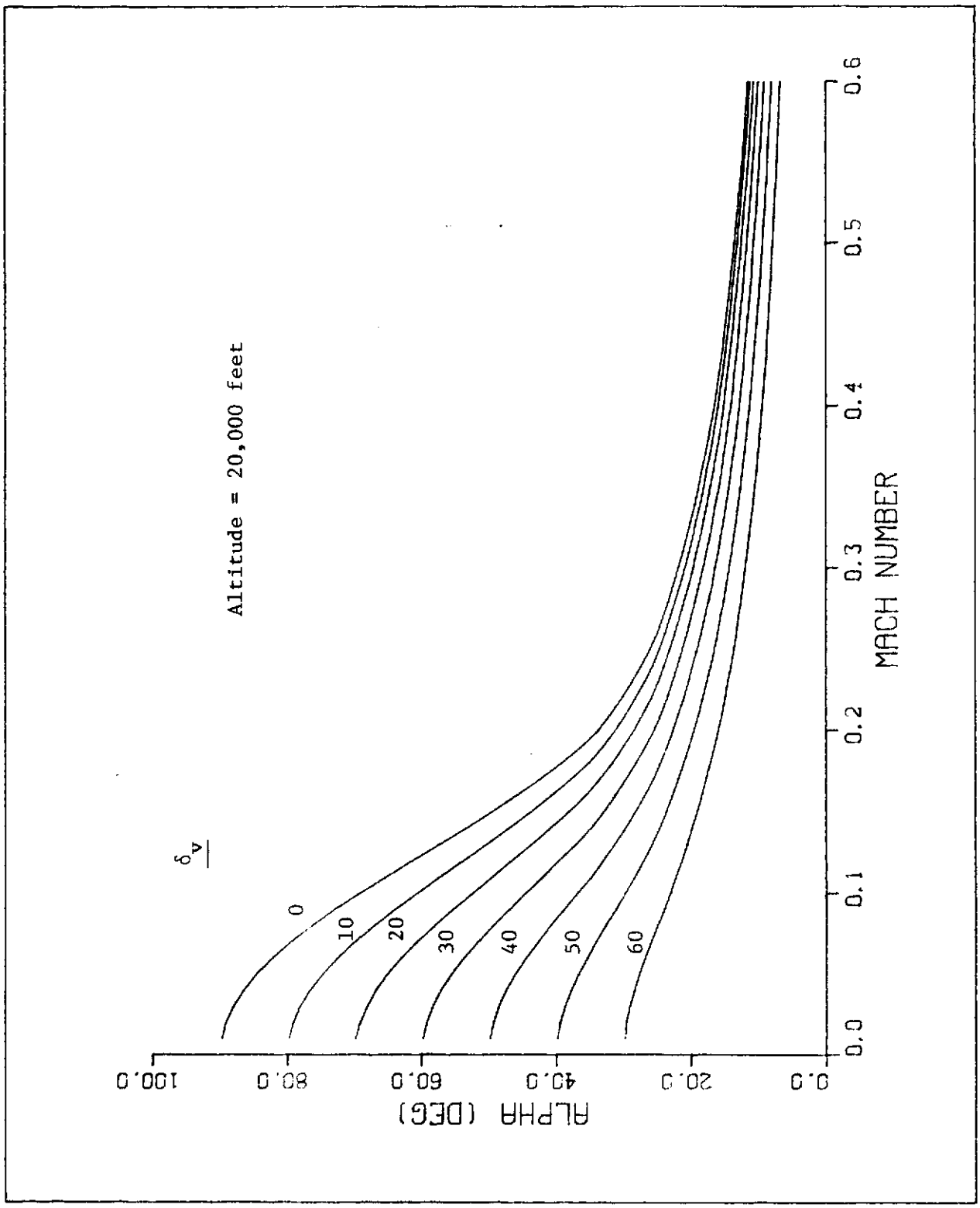

FIGURE 17. Angle of Attack for Sustained Turning Rate as a Function of Thrust Vector Angle

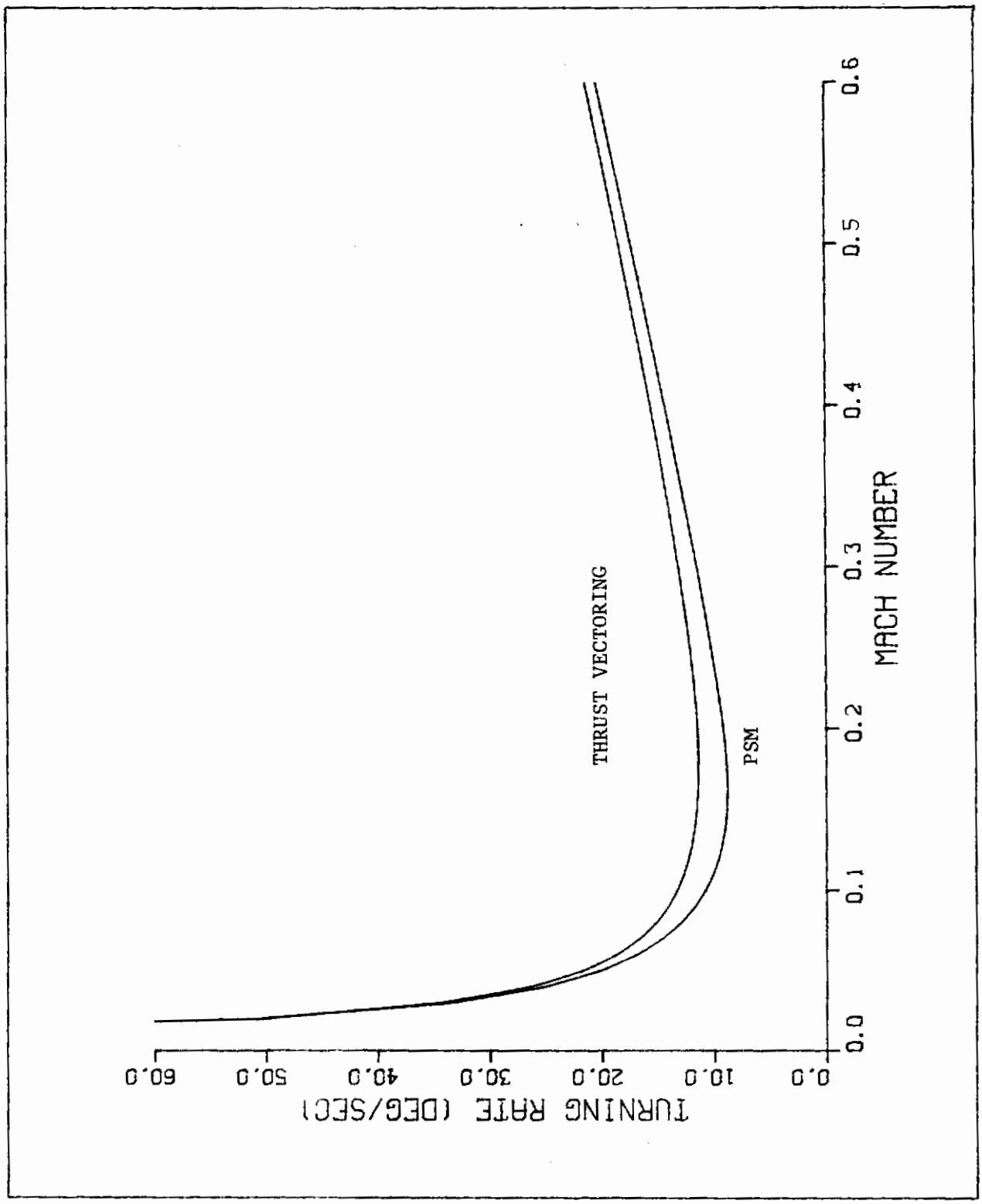

FIGURE 18. Maximum Turning Rates

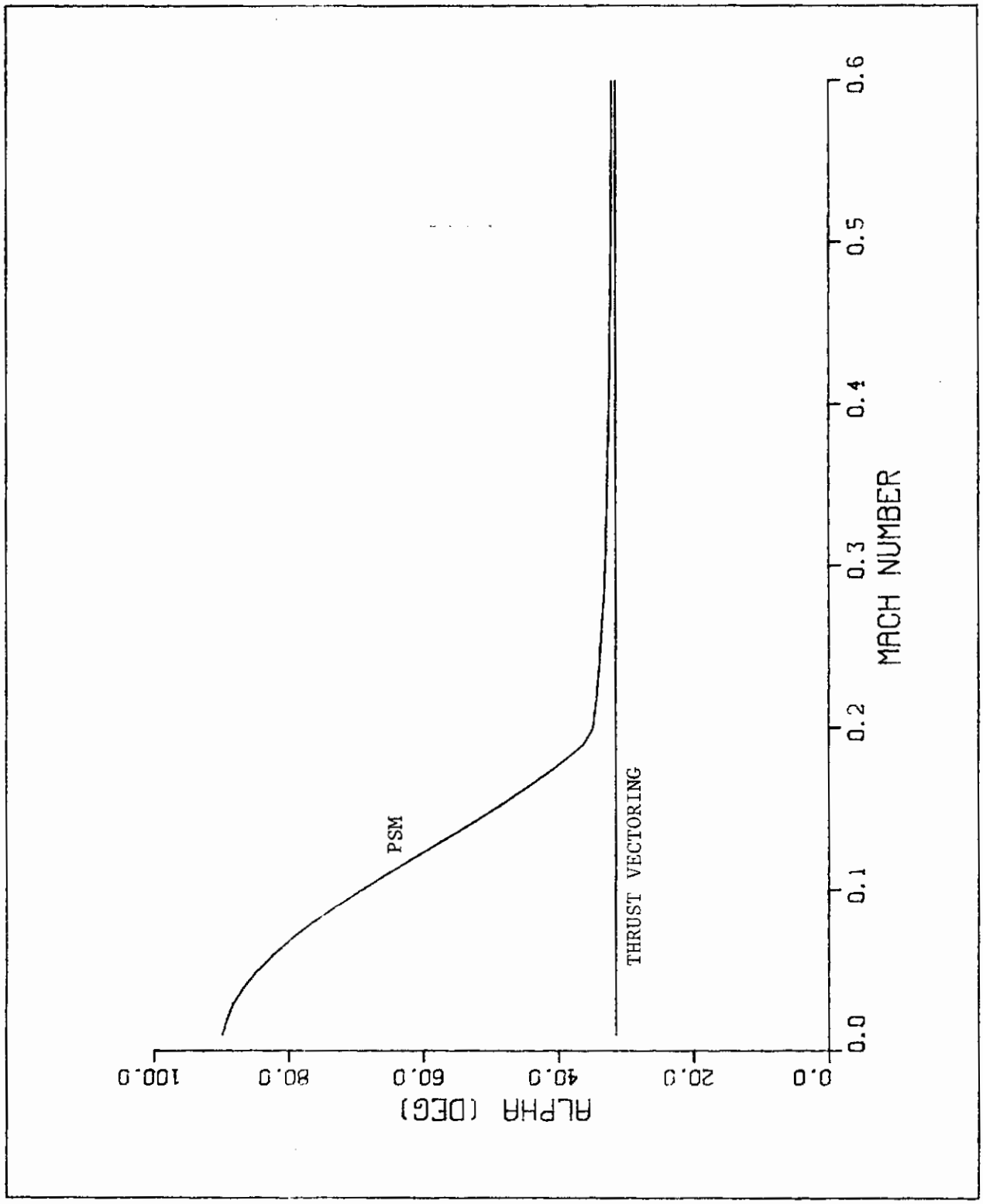

FIGURE 19. Optimal Angles of Attack

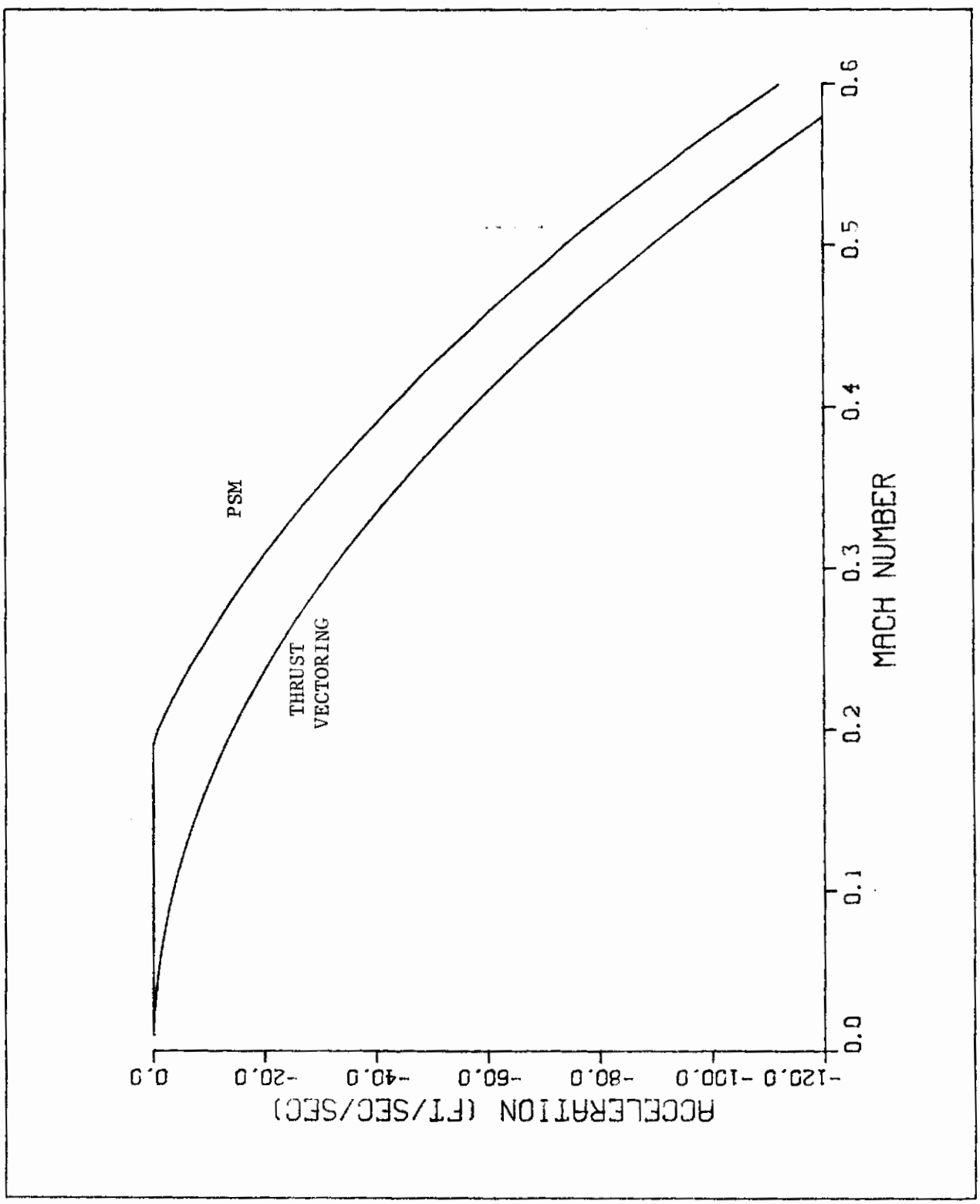

FIGURE 20. Longitudinal Acceleration

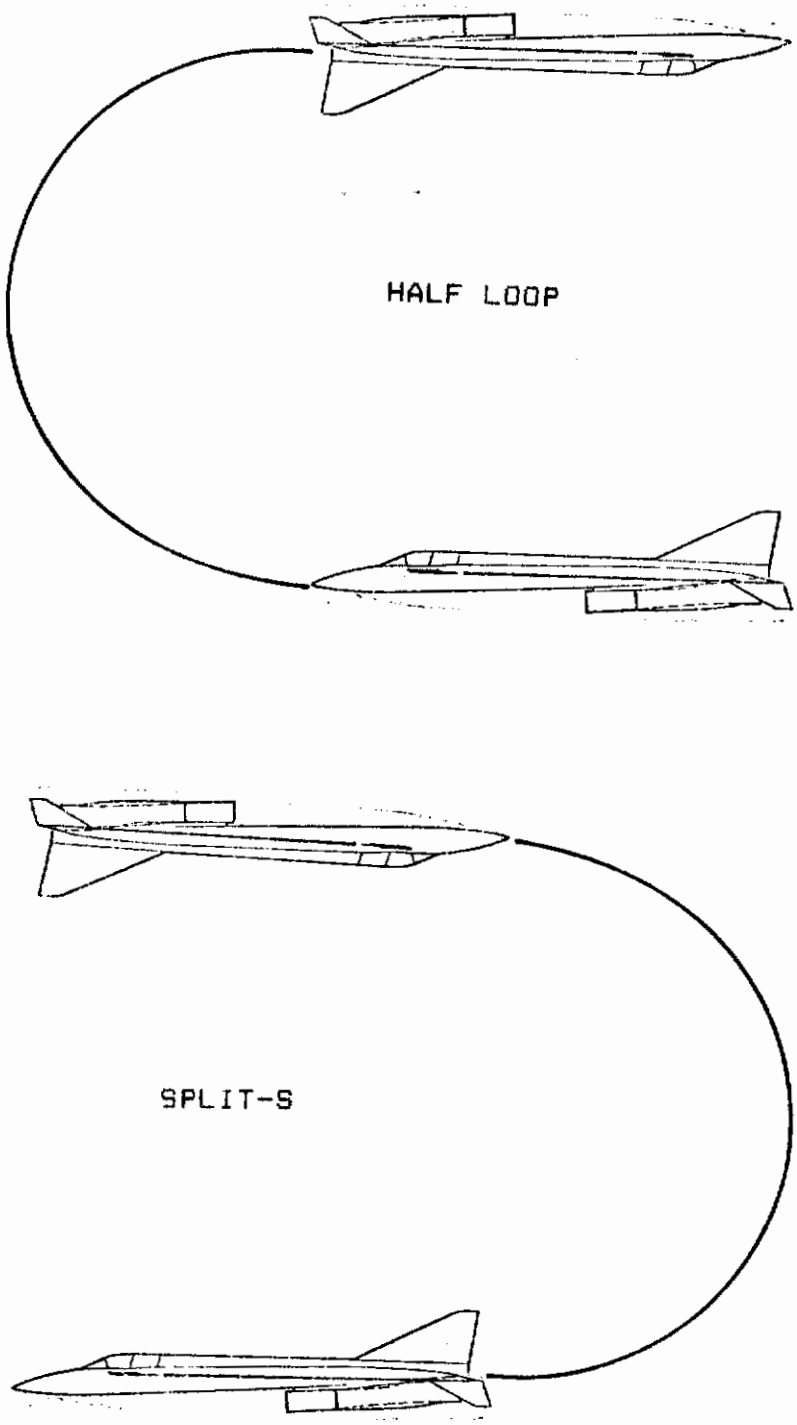

FIGURE 21. Vertical Plane Maneuvers

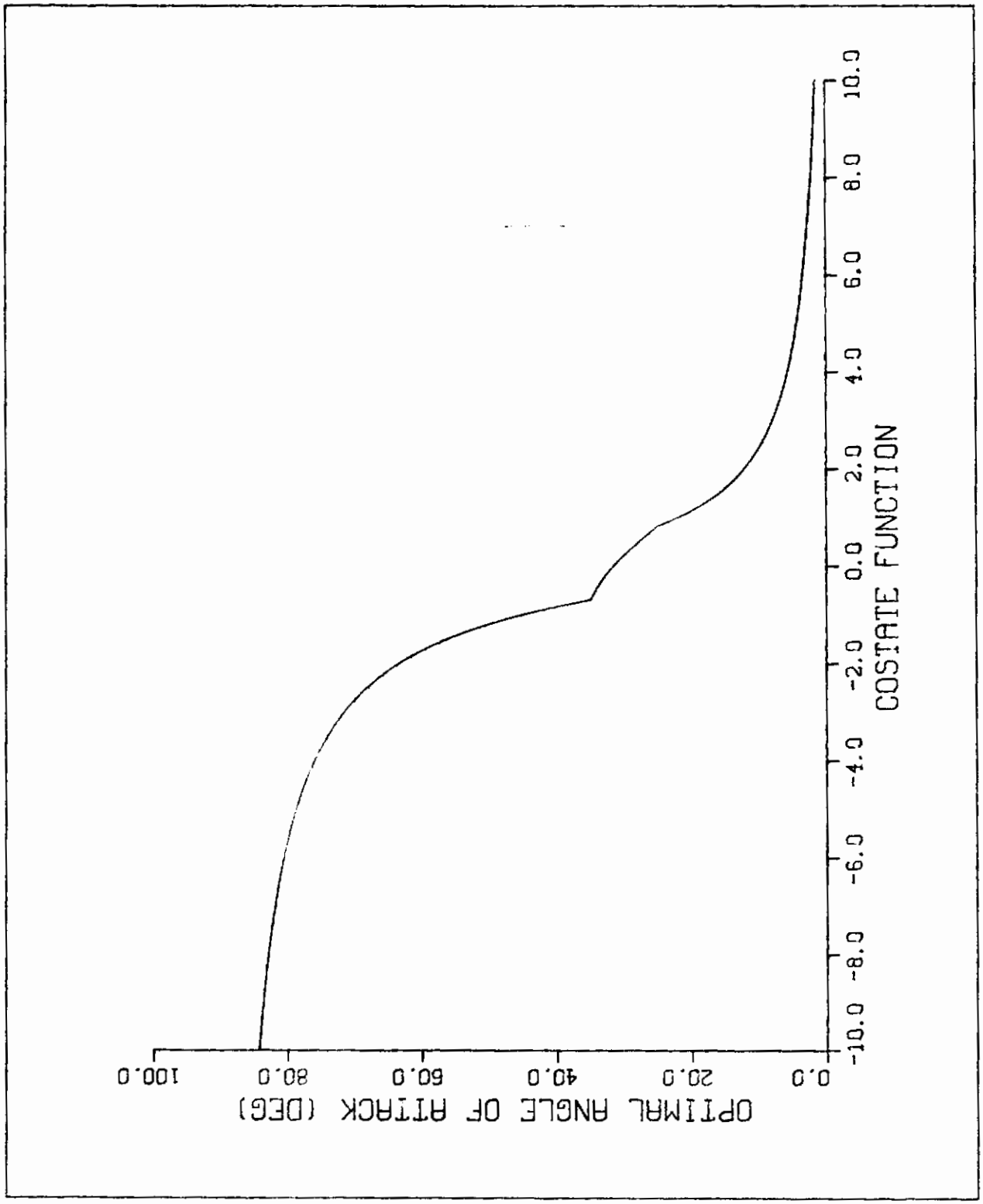

FIGURE 22. Optimal Angle of Attack as a Function of the Costate Function

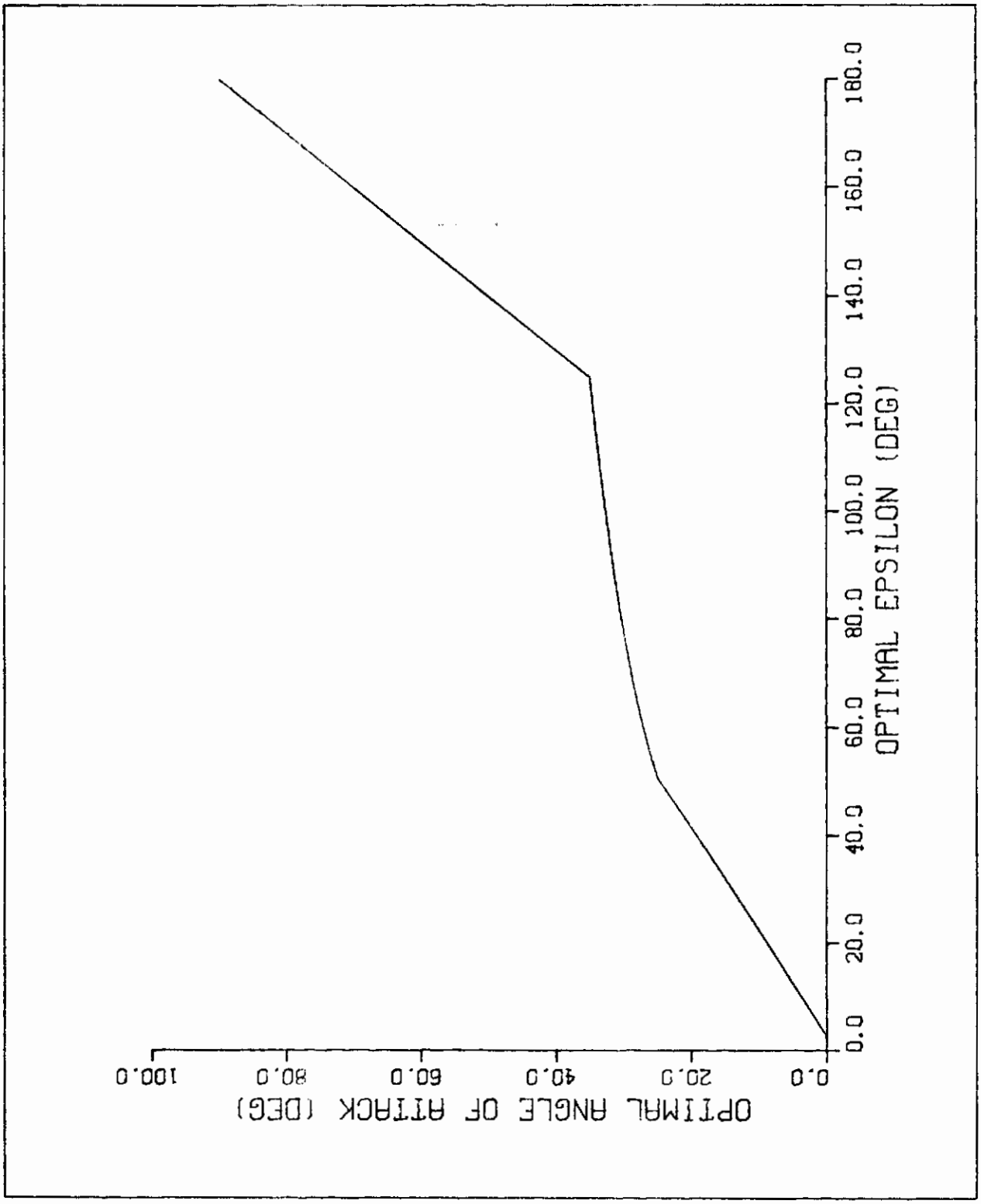

FIGURE 23. Optimal Angle of Attack as a Function of Optimal Epsilon

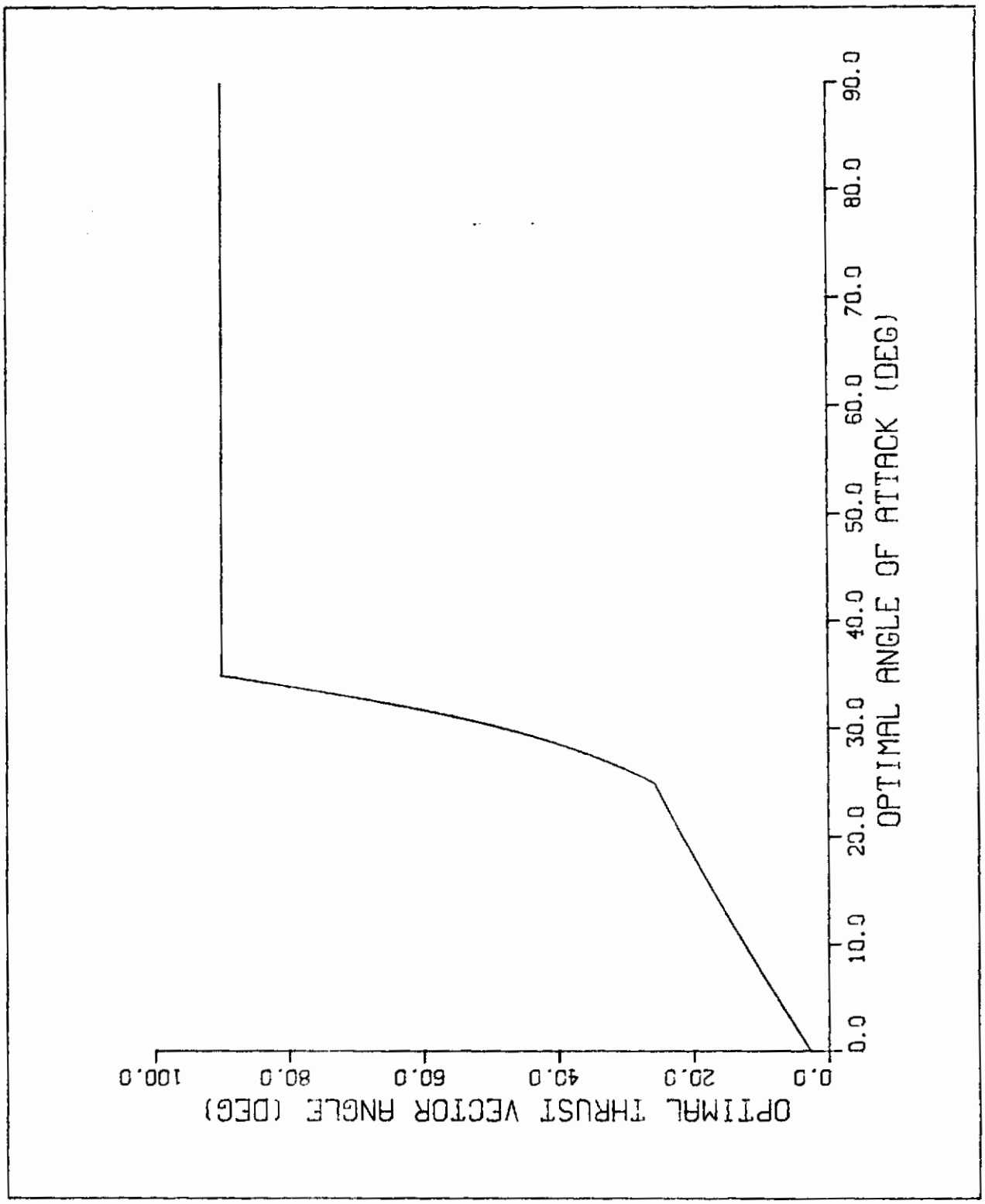

FIGURE 24. Optimal Thrust Vector Angle as a Function of the Optimal Angle of Attack

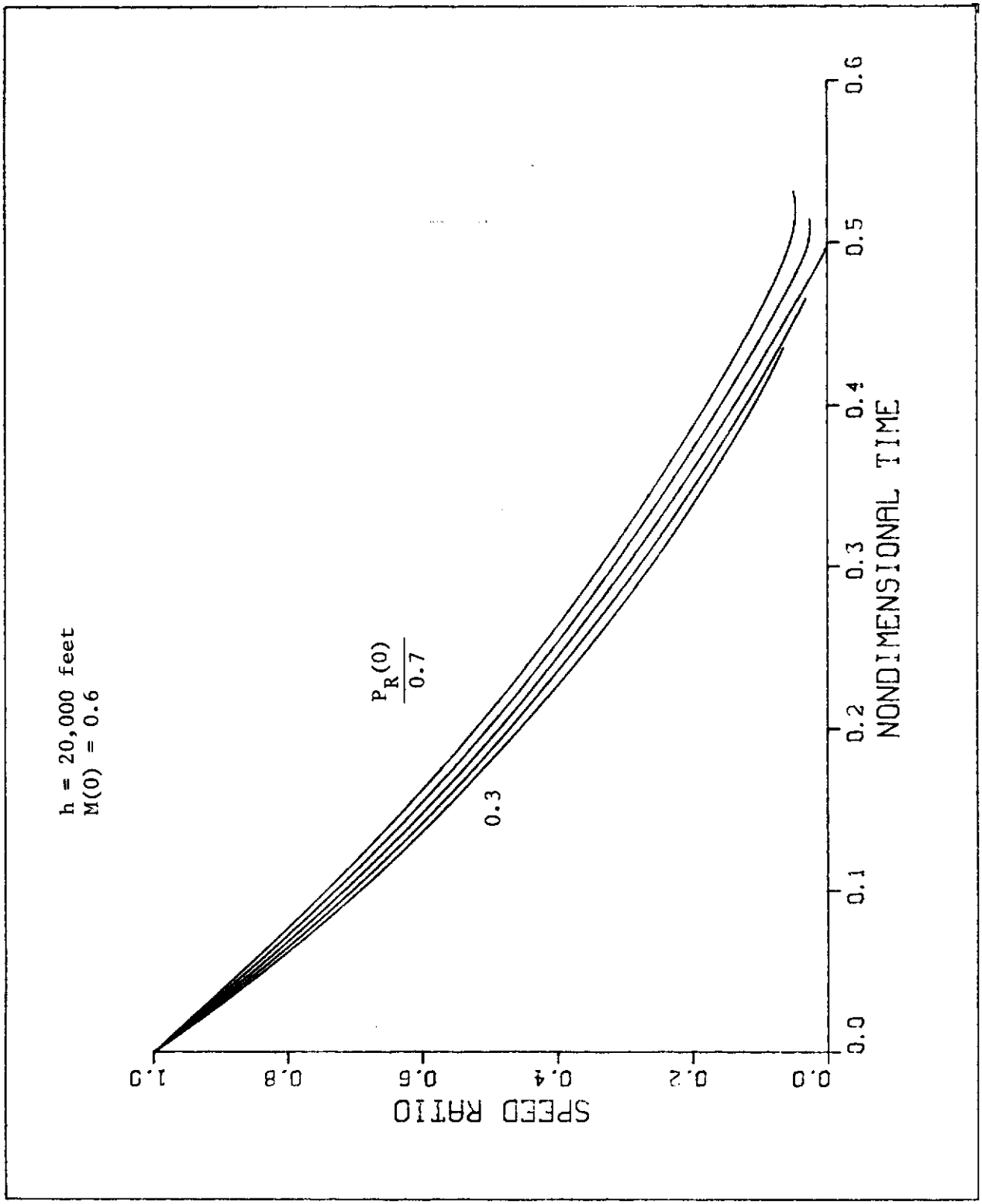

FIGURE 25. Speed Ratio

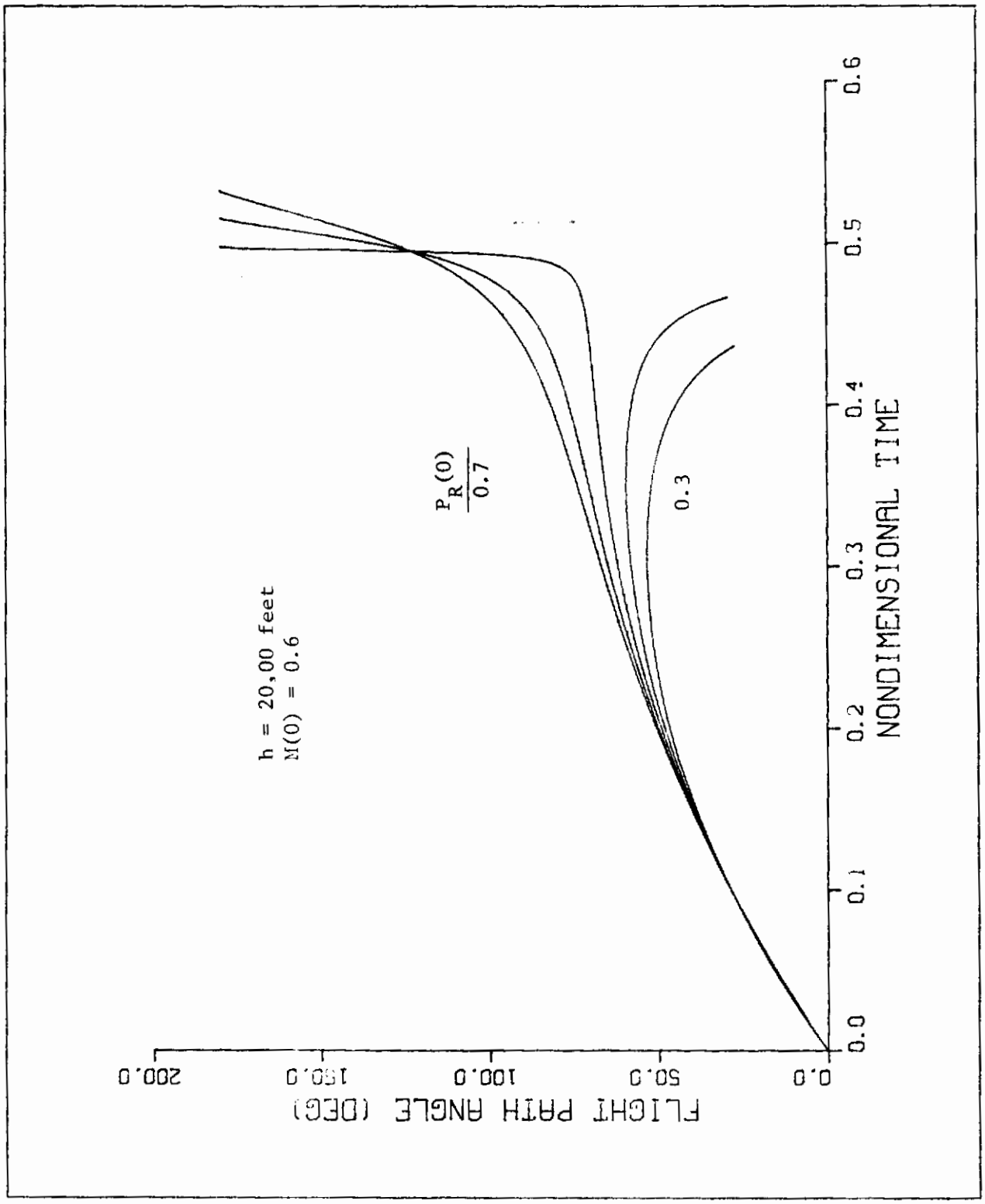

FIGURE 26. Flight Path Angle

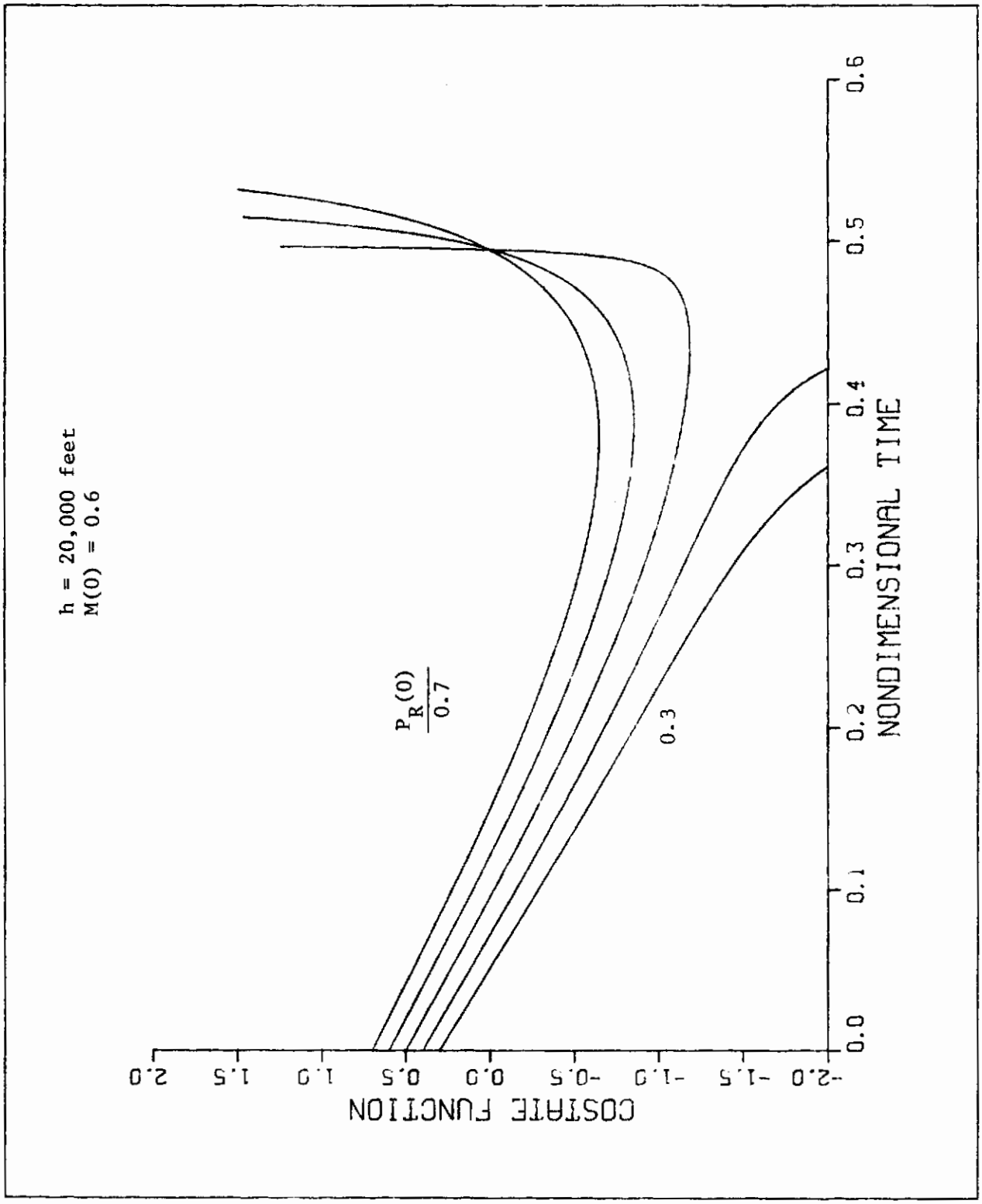

FIGURE 27. Costate Function

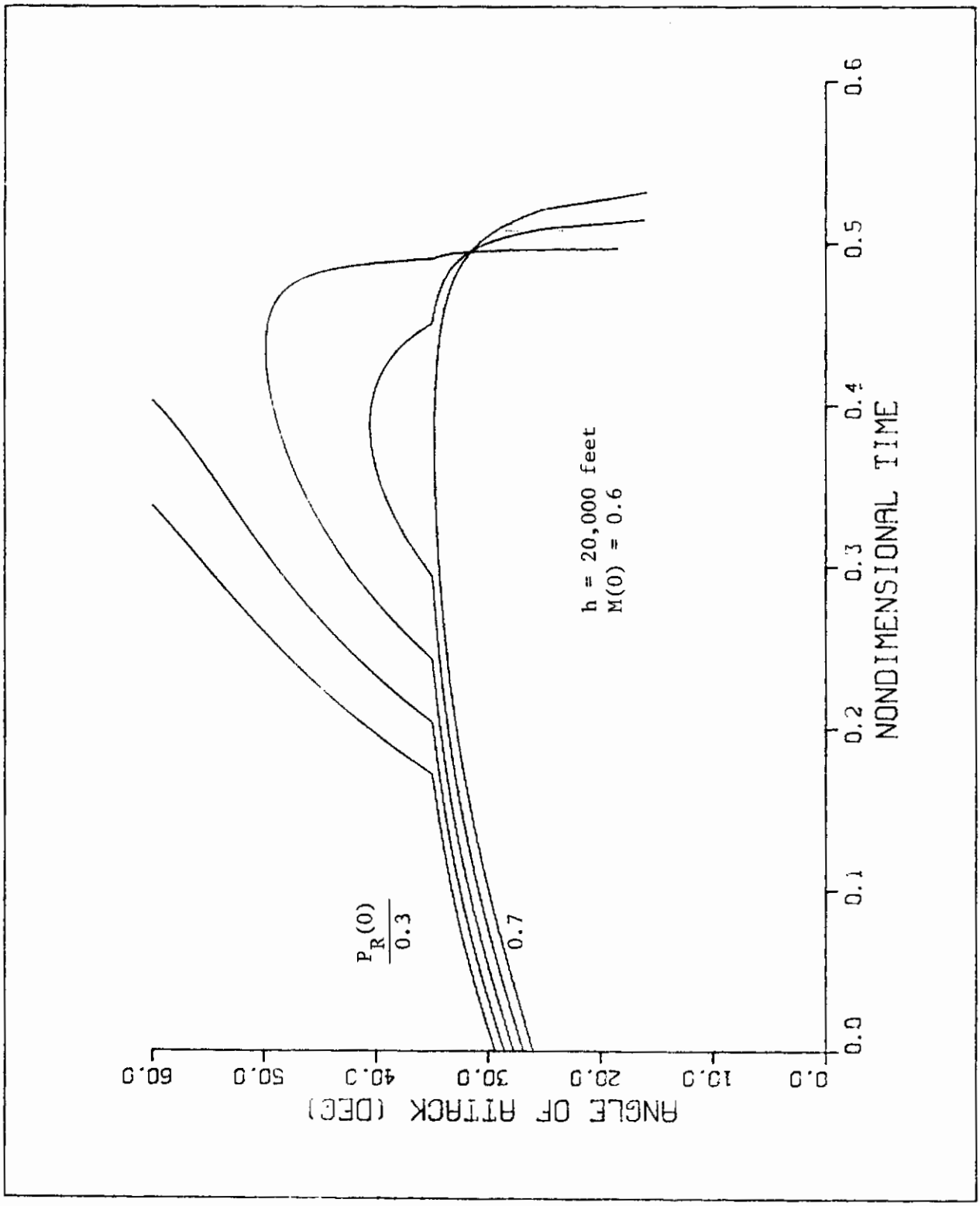

FIGURE 28. Angle of Attack

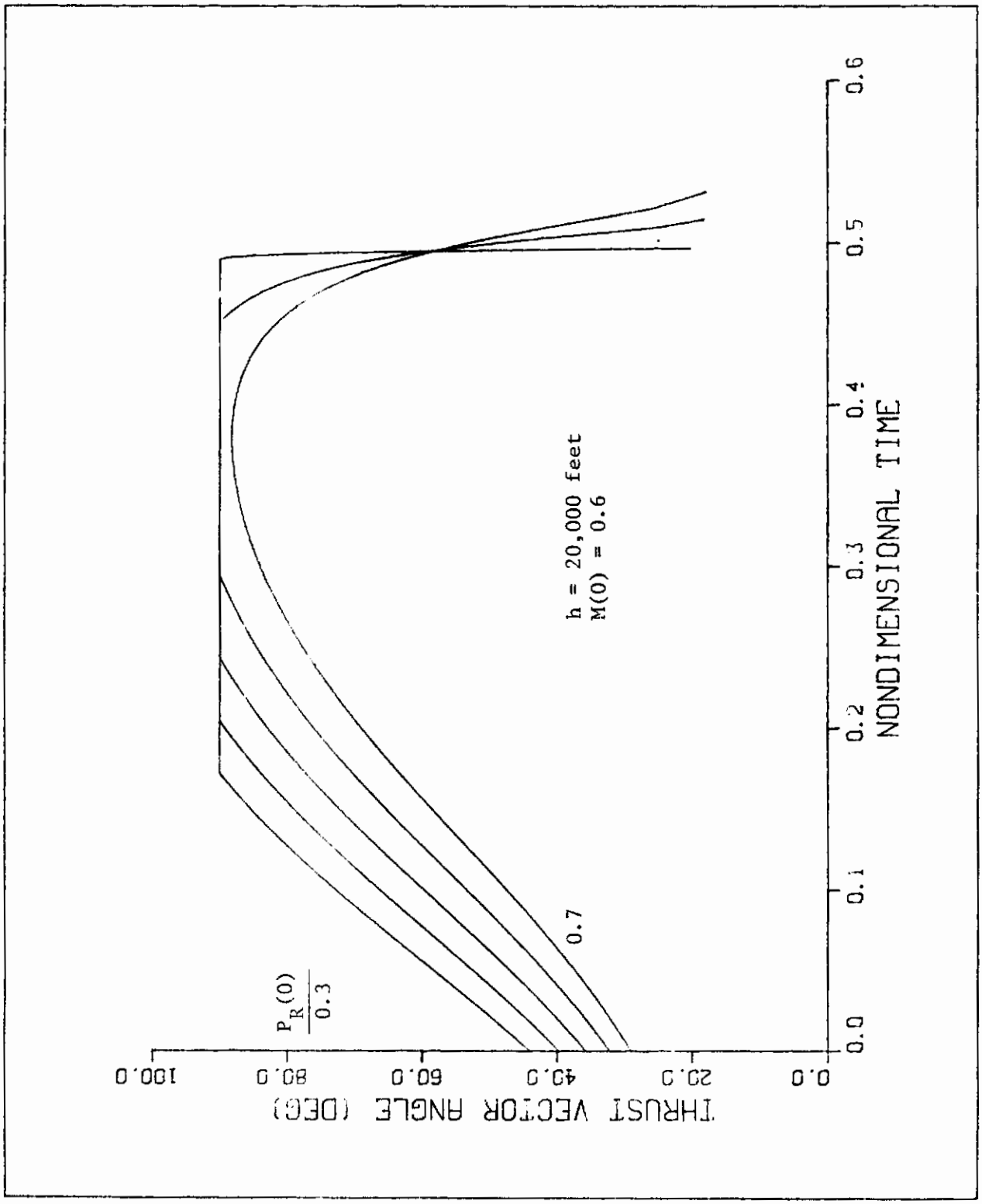

FIGURE 29. Thrust Vector Angle

* U.S.Government Printing Office: 1985 — 559-065/20856